國立臺灣大學工學院化學工程學系

碩士論文

Department of Chemical Engineering

College of Engineering

National Taiwan University

Master Thesis

考量初級成核之晶種與非晶種批次結晶製程之最適化

Optimization of Seeded and Unseeded Batch Crystallization

Processes with Primary Nucleation

簡瑋廷

Wei-Ting Chien

指導教授：吳哲夫 博士

Advisor: Jeffrey D. Ward, Ph.D.

中華民國 112 年 6 月

June, 2023

國立臺灣大學碩士學位論文
口試委員會審定書

考量初級成核之晶種與非晶種批次結晶製程之最適化

Optimization of Seeded and Unseeded Batch Crystallization
Processes with Primary Nucleation

本論文係簡瑋廷君（學號 R10524013）在國立臺灣大學化學工程學系完成之碩士學位論文，於民國 112 年 6 月 8 日承下列考試委員審查通過及口試及格，特此證明

口試委員：

_____（簽名）
（指導教授）

_____   _____

_____   _____

系主任、所長 _____（簽名）

（是否須簽章依各院系所規定）

i

誌謝

首先感謝我的指導教授吳哲夫教授(Jeffrey Ward)，從大四以來的悉心指導與鼓勵，在面臨研究瓶頸時為我指點迷津，適時的引導讓我能夠順利度過難關。也感謝教授一直以來的信任，給予學生相當大的空間，能夠自由規劃時間、自主安排研究方向與進度。另外，也感謝錢義隆教授、陳誠亮教授與余柏毅教授，在每學期大咪報告上給予的建議與回饋，使本論文至臻完善。

除此之外，還要特別感謝李豪業教授與吳哲夫教授，讓我有機會執行業界產學合作案，感謝兩位教授、晧人學長、銘君學長與世昌學長，在產學合作期間提供的建議與指導。不論是化工製程、類神經網路模型的學習，或與廠區的溝通、合作技巧，皆是彌足珍貴的經驗，相信未來在職場中將使我受益無窮。

接著要感謝實驗室的各位。謝謝晧人學長帶領我進入結晶領域，為我奠定紮實的理論基礎，也時常與我討論實驗結果、提供建議，協助我順利完成研究，即便學長如今已踏入職場，在繁忙的工作之餘仍不厭其煩為我解惑。謝謝采薇學姐、銘君學長、聰偉學長在研究及課業上的協助，並辛苦處理實驗室大大小小的事務。謝謝槃昕、衡山、至寬、孟暐兩年來共患難、互相幫助，閒暇時打球、聊天轉換心情，放鬆後再重新投入研究。謝謝其他同學、學弟妹讓實驗室充滿歡笑，良好的氣氛讓大家都能安心、愉快的作研究。

最後，感謝家人一路以來的支持，讓我沒有後顧之憂，能夠潛心研究。也感謝男友宜成多年的陪伴與鼓勵，是我的心靈慰藉與支柱。很高興終於完成碩士學業，謝謝大家一路相伴，讓我的碩士生活多采多姿。畢業，是結束，亦是嶄新的開始，我將邁向下一段旅程持續奮鬥，續寫人生新篇章。

中文摘要

　　本研究開發了一個框架來解決晶種和非晶種批次結晶系統最適化問題。在本研究中，應用最佳控制理論(optimal control theory)來求解考量初級成核之多目標批次結晶製程最適化問題，本論文陳述並求解晶種與非晶種之最適化問題，同時也追蹤成核晶體的質量，並將其包含在質量平衡中。然而由此產生的兩點邊界值問題(two-point boundary value problem)非常複雜，狀態(states)及協態(costates)變數的導數表達式為高度非線性的，因此傳統的打靶法(shooting method)往往難以收斂。在含有晶種的案例中，可透過假設在哈密頓(Hamiltonian)方程式中成核的質量相較於晶種成長的質量是可忽略不計的，來簡化數學計算。而在非晶種的案例中，可應用基於梯度(gradient-based)的演算法來有效地求解兩點邊界值問題。

　　本論文以氨苄青黴素(ampicillin)在水中析出結晶為個案研究，展示本論文中所提出的最佳化方法，進而求得最佳控制輸入曲線(如過飽度軌跡、pH 值軌跡)。本研究亦透過建構柏拉圖最佳解前緣(Pareto-optimal front)來分析不同目標函數間的競爭權衡關係，如最小化成核晶體數量、成核質量，或最大化晶體之加權平均大小。本研究所提出之演算法快速且穩健，或許可適用於模型基底線上控制。除此之外，此演算法未來也可用於解決更複雜之批次結晶系統之最適化問題。

關鍵字：初級成核；模型基底控制；粒數平衡方程式；多目標最佳化；最佳控制理論

ABSTRACT

This work develops a framework for solving optimization problems for both seeded and unseeded batch crystallization systems. In this work, optimal control theory (OCT) is applied to solve multi-objective optimization problems for batch crystallization processes with primary nucleation. Optimization problems for both seeded and unseeded cases are stated and solved. The mass of the nucleated crystals is tracked and included in the material balance. The resulting two-point boundary-value problems (TPBVPs) are difficult to solve because the expressions for the derivatives of the states and costates are highly non-linear. Conventional shooting methods usually fail to converge. In seeded case, the nucleus-grown mass in the Hamiltonian equation is assumed to be negligible compared to the seed-grown mass, which simplifies the mathematics. In unseeded case, a gradient-based algorithm is applied to solve the TPBVP efficiently.

A case study of ampicillin crystallized from water illustrates the method developed in this work. Optimal control input profiles (e.g. supersaturation trajectories and pH trajectories) and the complete product CSD are determined. Furthermore, the Pareto-optimal fronts are constructed to analyze the trade-off between the competing objectives of minimizing the number of nucleated crystals and the nucleated mass or the weight mean size. The algorithm is found to be both fast and robust, suggesting that it might be suitable for online model-based control. Moreover, the algorithm proposed in this work

might be useful for solving even more complicated optimization problems for batch crystallization systems with complex kinetics.

CONTENTS

LIST OF FIGURES

LIST OF TABLES

x

Chapter 1 Introduction

1.1   Overview of Crystallization Processes

Crystallization is a critically important separation process in many industries, including pharmaceuticals, specialty chemicals and food. Crystallization can proceed in either continuous or batch-wise. Continuous crystallization has the advantages of larger production rate and lower operating and capital cost[1-4]. Batch crystallization is simpler and more flexible, but batch-to-batch variability is a critical problem [5]. Both of them are common in industry; batch crystallization is the focus of this work.

In crystallization, the driving force is the supersaturation, which means that a solution contains more solute than the equilibrium solubility allows. Several methods can be used to induce supersaturation, such as cooling, evaporation of solvents, and changing the pH value[6]. Figure 1.1 shows three different common supersaturation trajectories [7]. Early growth trajectory represents that supersaturation is highest in the beginning, and is decreasing during the batch. The characteristic of late growth trajectory is that supersaturation is increasing with the batch time, and reaches the maximum in the end. The choice between these two operating policies will be discussed in Section 3.1.1. The third type of trajectories, constant supersaturation, is a heuristic operating policy when optimization is not available. It has been found to be much better than the uncontrolled

case, such as natural cooling. The constant supersaturation control will be discussed in

Section 1.2.
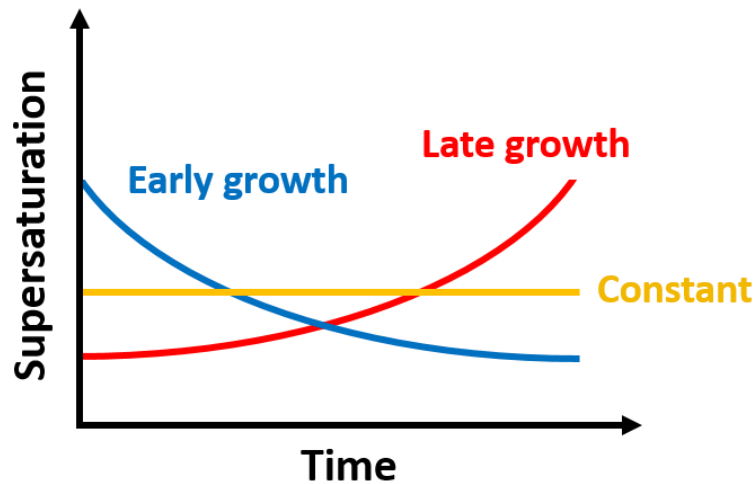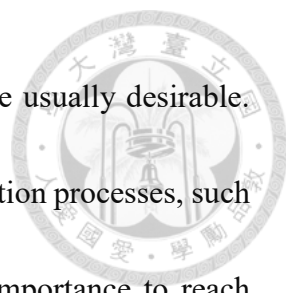
Figure 1.1. Common supersaturation trajectories: early growth, late growth, and

constant supersaturation[7].

Basic crystallization mechanisms consist of nucleation[8] and crystal growth[9; 10].

Nucleation represents the birth of new nuclei, and crystal growth stands for the increment

of the crystal size. In addition, nucleation can be divided into primary and secondary

nucleation. The former occurs in the absence of crystals, and the latter is induced by

parent crystals, which act as a site for the generation of new nuclei[11].

Crystal size distribution (CSD) is often an important measure of product quality

because it can influence downstream unit operations such as filtration or drying and

product properties including bioavailability, tabletability bulk flow, rate of dissolution,

2

etc[12; 13]. Large crystal mean size, narrow and unimodal CSD are usually desirable. Moreover, because high valuable products are produced in crystallization processes, such as food additives and pharmmaceuticals, optimization is of great importance to reach desired product properties. This work focuses on the optimization of batch crystallization processes.

1.2   Literature Review and Motivation

As mentioned in Section 1.1, CSD is highly related to product quality. Therefore, several control strategies have been proposed to achieve a desired CSD[14], larger crystal size[15; 16], or higher productivity[17]. Model-free control is simpler to design compared to model-based control because complicated mathematical models are not required. Direct nucleation control (DNC) is a widely used model-free feedback control approach. Information about the number of particles is obtained from the number of counts per seconds recorded by a focused beam reflectance measurement (FBRM)[14; 18] instrument, and transmitted to the controller. Cycles of cooling and heating can be conducted to achieve a desired CSD with fewer nucleated crystals. It has been shown that DNC can effectively reduce batch-to-batch variability in batch crystallization, and can help reject disturbances in continuous process[19]. Constant supersaturation control (SSC) is another common control strategy because of its simplicity. Attenuated total reflection-

Fourier-transform IR (ATR-FTIR)[20] or attenuated total reflection-ultraviolet/visible (ATR-UV/vis) spectroscopy[21] can be used to measure the concentration continuously to implement the feedback control of supersaturation. The concentration is first measured and used to compare the supersaturation with its set point. A signal will then be sent to the temperature controller, and the constant supersaturation can be maintained by manipulating the temperature of the crystallizer. In model-free control, crystallization kinetics and modeling are not required, and parameter uncertainty no longer plays a role, especially the stochastic phenomenon of primary nucleation. Although model-free control provides a simple and rapid process design, it might be suboptimal, and direct design of the product CSD is not available[22].

Therefore, model-based control is also of great interest. Population balance equation (PBE), which is a partial differential equation including population density function, crystal growth rate and nucleation rate, is used to calculate the time evolution of CSD. Mesbah et al.[17] obtained an optimal growth rate profile for ammonium sulphate-water system by using a model-based controller to maximize the batch productivity subject to the product quality requirements. Nagy[23] proposed a model-based robust control approach for batch crystallization to determine optimal temperature and concentration trajectories, aiming to achieve a desired CSD shape subject to the operating constraints.

However, solving PBE for model-based design is sometimes challenging because it is a partial differential equation and analytical solutions usually do not exist. One option is to solve the problem numerically by discretization of the CSD. Methods that take this approach include the method of characteristics[24; 25], finite difference methods[26], and Monte Carlo methods[27; 28]. Using these methods, the complete CSD can be determined but discretization methods are computationally intensive. Another well-known numerical approach, the method of moment (MOM)[29-31], does not require discretization of the CSD. By applying MOM, the PBE can be converted to a series of ordinary differential equations, which simplifies the calculation. Although MOM is computationally efficient, in general complete information about the CSD cannot be obtained.

Raisch and coworkers[32-36] proposed a time transformation that may simplify the solution of PBEs. Hofmann and Raisch further showed that nearly analytical solutions to certain optimization problems can be obtained by Pontryagin's Minimum Principle (PMP) [37; 38] if the feedback of nucleated crystal mass is neglected[39]. Using this framework, several problems in optimization of seeded batch crystallization processes have been solved[40-44]. The method has been found to be very accurate and computationally efficient.

Based on the framework proposed by Raisch and coworkers [32-36], optimization problems for seeded batch crystallization processes with negligible primary nucleation

5
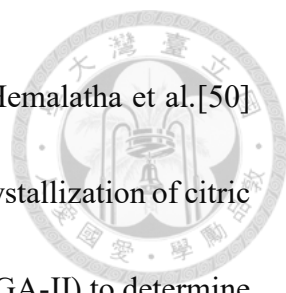
have been widely studied, including multivariate systems,[32; 34] systems with size-independent[39] and size-dependent[41] growth rate kinetics, and systems considering crystal shape[43]. Design of seed recipe[42] and trade-off between different objective functions[40; 44] have also been studied.

To our knowledge, all previous studies based on the transformation proposed by Raisch and coworkers have been of systems where seeds are present, secondary nucleation dominates over primary nucleation, and the nucleus-grown mass is small enough that it can be neglected compared to the seed-grown mass in the overall mass balance. These assumptions simplify the mathematics and in some cases make a nearly-analytical solution possible.

Although seeds are often used in batch crystallization processes to control the CSD by inhibiting nucleation, and seeding policy has also been studied[42; 45], seeding is not without disadvantages[46-49]: It is difficult to maintain sterility when adding seeds and impurities including bacteria may be introduced. Toxic organic solvent vapors may escape the crystallizer when seeds are added. Seeds may aggregate and disperse poorly in the crystallizer. Finally, seed properties such as purity, polymorph and surface properties may vary from batch to batch resulting in variable batch quality.

Considering that seed preparation is challenging due to the requirement of high-quality seeds, unseeded crystallization is also of great importance. However, less research

has focused on the optimization of unseeded batch crystallization. Hemalatha et al.[50] applied multi-objective optimization to the unseeded batch cooling crystallization of citric acid anhydride using a non-dominated sorting genetic algorithm (NSGA-II) to determine the optimal cooling trajectory. Ashraf and Rao[51] also applied NSGA-II to carry out multi-objective optimization for unseeded batch cooling crystallization of aspirin, and determined optimal temperature trajectory.

It is of interest to determine whether the transformation of Raisch, which has been applied successfully to problems with seeds and secondary nucleation, can also be applied in cases where primary nucleation is significant and to cases where seeds are not used. That is the purpose of this work. Relaxing these restrictions results in a significant complication of the problem and in the latter case requires a nearly complete reformulation of the problem because there is no longer an algebraic relationship between the transformed time and the solid mass in the crystallizer. Nevertheless in this work we show that these generalized optimization problems can be formulated and solved efficiently using a gradient-based algorithm[52-54] to solve the associated two-point boundary-value problem.

1.3　Thesis Organization

The remainder of this thesis is organized as follows. In Chapter 2, population balance

models and crystallization kinetic models are presented. In Chapter 3, optimization

problems are formulated for both seeded and unseeded cases. A case study presented in

Chapter 4 illustrates the framework developed in this work, and the optimal operating

trajectories and other results are presented and compared for each case. Finally,

conclusions are given in Chapter 5.

Chapter 2 Theory

In this chapter, theory of modeling of batch crystallization processes is presented in Section 2.1, and the crystallization kinetics are introduced in Section 2.2.

2.1 Modeling of Batch Crystallization Processes

For a batch crystallization process in a well-mixed crystallizer, if crystal breakage and aggregation are neglected, and nuclei form with zero size, then the PBE can be written:

$$\frac{\partial f(t,L)}{\partial t} + G(t)\frac{\partial f(t,L)}{\partial L} = B(t)\delta(L) \tag{2.1}$$

$$f(0,L) = f_{\text{ini}}(L) \tag{2.2}$$

where f is the population density function depending on process time t and crystal size L, f_{ini} is the initial CSD, G is the size-independent linear growth rate, δ is a Dirac delta function, and B is the nucleation rate.

Eq 2.1 is a partial differential equation which can be difficult to solve. The MOM[31] can be applied to simplify the calculations. Define the ith moment of the CSD μ_i as

$$\mu_i = \int_0^\infty L^i f(L)dL, i = 0,1,2,\ldots \tag{2.3}$$

Eq 2.1 can be converted to the following set of ordinary differential equations:
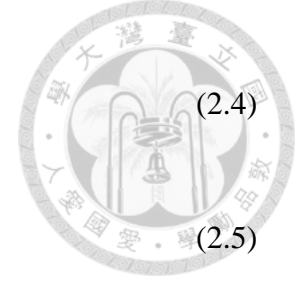
$$\frac{d\mu_0}{dt} = B \qquad (2.4)$$

$$\frac{d\mu_i}{dt} = iG\mu_{i-1}, i = 1,2,3 \dots \qquad (2.5)$$

A new time variable τ is introduced[32-36] and defined as

$$d\tau = G(t)dt; \tau(t = 0) = 0 \qquad (2.6)$$

where τ has units of length. Eq 2.4 and Eq 2.5 can then be written as

$$\frac{d\mu_0}{d\tau} = \frac{B}{G} \qquad (2.7)$$

$$\frac{d\mu_i}{d\tau} = i\mu_{i-1}, i = 1,2,3 \dots \qquad (2.8)$$

For unseeded crystallization, the initial conditions of Eq 2.7 and Eq 2.8 are

$$\mu_i(0) = 0, i = 0,1,2 \dots; \quad t(0) = 0 \qquad (2.9)$$

For seeded crystallization, the ith moment of the CSD μ_i can be divided into two

parts: $\mu_{i,s}$ and $\mu_{i,\mathrm{n}}$ representing the ith moment of the seed-grown and nucleus-grown

crystals, respectively. At each point in time the ith moment of total crystals μ_i is the

sum of $\mu_{i,s}$ and $\mu_{i,\mathrm{n}}$. The corresponding ODEs and initial conditions are

$$\frac{d\mu_{0,\mathrm{s}}}{d\tau} = 0 \qquad (2.10)$$

$$\frac{d\mu_{i,\mathrm{s}}}{d\tau} = i\mu_{i-1,\mathrm{s}}, i = 1,2,3 \dots \qquad (2.11)$$

$$\frac{d\mu_{0,\mathrm{n}}}{d\tau} = \frac{B}{G} \qquad (2.12)$$

10

$$\frac{d\mu_{i,\mathrm{n}}}{d\tau} = i\mu_{i-1,\mathrm{n}}, i = 1,2,3\ldots \tag{2.13}$$

$$\mu_{i,\mathrm{s}}(0) = \mu_{i0,\mathrm{s}}, i = 0,1,2\ldots; \quad \mu_{i,\mathrm{n}}(0) = 0, i = 0,1,2\ldots; \quad t(0) = 0 \tag{2.14}$$

where $\mu_{i0,\mathrm{s}}$ is the ith moment of seed crystals, which can be calculated from Eq 2.3.

In addition, Eq 2.10 and Eq 2.11 can be directly integrated to obtain each moment

of the seed-grown crystals as a function of τ:

$$\mu_{0,\mathrm{s}}(\tau) = \mu_{00,\mathrm{s}} \tag{2.15}$$

$$\mu_{1,\mathrm{s}}(\tau) = \mu_{00,\mathrm{s}}\tau + \mu_{10,\mathrm{s}} \tag{2.16}$$

$$\mu_{2,\mathrm{s}}(\tau) = \mu_{00,\mathrm{s}}\tau^2 + 2\mu_{10,\mathrm{s}}\tau \tag{2.17}$$

$$\mu_{3,\mathrm{s}}(\tau) = \mu_{00,\mathrm{s}}\tau^3 + 3\mu_{10,\mathrm{s}}\tau^2 + 3\mu_{20,\mathrm{s}}\tau + \mu_{30,\mathrm{s}} \tag{2.18}$$

This transformation can also be applied to Eq 2.1.The PBE becomes:

$$\frac{\partial f(\tau, L)}{\partial \tau} + \frac{\partial f(\tau, L)}{\partial L} = \frac{B}{G}(\tau)\delta(L) \tag{2.19}$$

For unseeded crystallization, the initial condition and the analytical solution are

$$f(0, L) = 0 \tag{2.20}$$

$$f(\tau, L) = \frac{B}{G}(\tau - L), \tau - L \geq 0 \tag{2.21}$$

For seeded crystallization, Eq 2.19 can be divided into two parts:

$$\frac{\partial f_s(\tau, L)}{\partial \tau} + \frac{\partial f_s(\tau, L)}{\partial L} = 0 \tag{2.22}$$

$$\frac{\partial f_n(\tau, L)}{\partial \tau} + \frac{\partial f_n(\tau, L)}{\partial L} = \frac{B}{G}(\tau)\delta(L) \tag{2.23}$$

where f_s and f_n are seed-grown and nucleus-grown population density function, respectively. The corresponding initial conditions and analytical solutions are

$$f_s(0, L) = f_{ini}(L) \tag{2.24}$$

$$f_n(0, L) = 0 \tag{2.25}$$

$$f_s(\tau, L) = f_{ini}(L - \tau), L - \tau \geq 0 \tag{2.26}$$

$$f_n(\tau, L) = \frac{B}{G}(\tau - L), \tau - L \geq 0 \tag{2.27}$$

2.2 Crystallization Kinetics

Only crystal growth, primary nucleation, and secondary nucleation are considered in this work. The expressions for the size- and temperature-independent linear growth rate G, primary nucleation rate B_1, and secondary nucleation rate B_2 used in this work are:

$$G = k_g(S - 1)^g \tag{2.28}$$

12

$$B_1 = k_{b1} \exp\left(\frac{-A}{(\ln(S))^2}\right) \qquad (2.29)$$

$$B_2 = k_{b2}(S-1)^b \mu_3^d \qquad (2.30)$$

where k_g, k_{b1}, A, k_{b2}, g, b and d are constants. The total nucleation rate is the sum

of primary and secondary nucleation rates, i.e. $B = B_1 + B_2$. G, B_1, and B_2 depend on

the supersaturation S, and B_2 is also dependent on μ_3. Supersaturation S is defined as

$$S = \frac{C(t)}{C_{\text{sat}}} \qquad (2.31)$$

$$C(t) = C_{\text{ini}} - \rho k_V(\mu_3(t) - \mu_3(0)) \qquad (2.32)$$

where $C(t)$ is the concentration of the solution, C_{sat} is the saturation concentration,

C_{ini} is the initial concentration, ρ is the density of the crystals, and k_V is the volume

shape factor.

Chapter 3 Optimization Problems and Solutions

In this chapter, optimization problems are formulated in Section 3.1, including seeded and unseeded case. Pareto-optimal fronts are introduced in Section 3.2, and the objective function of each case is defined. Solutions to optimization problems for each case are presented in Section 3.3.

3.1   Optimization Problem Statements

For crystallization processes, optimization problems are solved to find optimal supersaturation trajectories. Each optimization problem includes an objective function to be minimized and relevant constraints.

3.1.1   Case 1: Seeded Crystallization

In seeded crystallization, nucleated crystals are usually undesirable because they broaden the product CSD. In this case, in the absence of constraints a very long batch time and a very small production rate will be preferable. Therefore constraints on the production rate and the batch time are set to ensure a reasonable solution.

The optimization problem for seeded crystallization with primary and secondary nucleation can be written:

$$\min_{S(\tau)} \quad \phi\big(\boldsymbol{\mu}(\tau_{\mathrm{f}})\big)$$

$$\text{s.t.} \quad \mu_{3,\mathrm{s}}(\tau_{\mathrm{f}}) = \mu_{3,\mathrm{s,c}}$$

$$t(\tau_{\mathrm{f}}) \le t_{\mathrm{f,c}}$$

$$S(\tau) \in (1, S_{\mathrm{ub}}] \tag{3.1}$$

where ϕ is the objective function, τ_{f} is the final transformed time, $\mu_{3,\mathrm{s,c}}$ is the constraint on the third moment of seed-grown crystals at the end of the batch, $t_{\mathrm{f,c}}$ is the batch time constraint in the time domain, and S_{ub} is the upper bound on the supersaturation. In this case, τ_{f} is fixed because it can be calculated from Eq 2.18 based on the production rate constraint $\mu_{3,\mathrm{s}}(\tau_{\mathrm{f}}) = \mu_{3,\mathrm{s,c}}$.

Both single-objective and multi-objective problems can be considered. Table 3.1 lists the common single objective functions considered in seeded crystallization processes[40]. The subscript f indicates the final properties of the product.

Table 3.1 Common single objective functions in seeded crystallization processes[40]

Objective	Definition
minimize the number of nucleated crystals	$\min \ \mu_{0,\mathrm{n,f}}$
minimize the volume of nucleated crystals	$\min \ \mu_{3,\mathrm{n,f}}$
maximize the number mean size	$\max \ \mu_{1,\mathrm{f}}/\mu_{0,\mathrm{f}}$
maximize the weight mean size	$\max \ \mu_{4,\mathrm{f}}/\mu_{3,\mathrm{f}}$
minimize the number mean coefficient of variation (number CV)	$\min \ \sqrt{\dfrac{\mu_{0,\mathrm{f}}\mu_{2,\mathrm{f}}}{\mu_{1,\mathrm{f}}^{2}} - 1}$
minimize the weight mean coefficient of variation (weight mean CV)	$\min \ \sqrt{\dfrac{\mu_{3,\mathrm{f}}\mu_{5,\mathrm{f}}}{\mu_{4,\mathrm{f}}^{2}} - 1}$

In seeded crystallization, inhibition of nucleation is usually the goal. Ward et al.[7] has summarized the choice of different objectives and the corresponding optimal

15

operating policies. In their work, it has been concluded that objectives involving the higher nucleus-grown moments would result in late growth operating policies, and that objectives involving lower nucleus-grown moments would result in early growth operating policies. Therefore, it is obvious that objectives involving higher nucleus-grown moments, such as $\mu_{3,n}$ and $\mu_{4,n}$, are competing with those involving lower nucleus-grown moments, such as $\mu_{0,n}$ and $\mu_{1,n}$. In this work, two competing objectives $\mu_{0,n,f} = \mu_{0,n}(\tau_f)$ (final number of nucleated crystals) and $\mu_{3,n,f} = \mu_{3,n}(\tau_f)$ (proportional to final volume of nucleated crystals) are often selected as the objectives to be minimized.

3.1.2 Case 2: Unseeded Crystallization

The optimization problem for unseeded crystallization can be written:

$$
\begin{aligned}
\min_{S(\tau),\tau_f} \quad & \phi\big(\boldsymbol{\mu}(\tau_f)\big) \\
\text{s.t.} \quad & \mu_3(\tau_f) = \mu_{3,c} \\
& t(\tau_f) \leq t_{f,c} \\
& S(\tau) \in (1, S_{ub}]
\end{aligned}
\tag{3.2}
$$

where $\mu_{3,c}$ is the final constraint on the third moment of crystals. For unseeded crystallization, the constraint on the production rate is different because all crystals are nucleus-grown ($\mu_{i,s} = 0, \ \mu_i = \mu_{i,n}$).

In this case, the goal is to produce larger but fewer crystals under the production rate constraint. Comparison of different objectives in unseeded crystallization has not been studied. Maximizing the number mean size ($\mu_{1,f}/\mu_{0,f}$), maximizing the weight mean size

16

$(\mu_{3,f}/\mu_{0,f})$, and minimizing the number mean coefficient of variation (min $\sqrt{\frac{\mu_{0,f}\mu_{2,f}}{\mu_{1,f}^2} - 1}$)

have been considered in the previous work[55; 56].
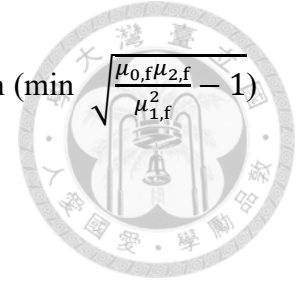
In unseeded crystallization, it is expected that minimizing the number of crystals would result in early growth operating policies because those crystals produced from nucleation in the beginning will have enough time to grow. Although it is difficult to predict the optimization result of maximizing the mean size of the product crystals, there might be a trade-off between the number and the mean size of the product crystals. Therefore, in this work, two single objectives are considered: minimize the final number of crystals ($\mu_{0,f} = \mu_0(\tau_f)$) or maximize the final weight mean size (WMS$_f$) of the crystals ($\mu_{4,f}/\mu_{3,f}$). Since the production rate constraint fixes $\mu_{3,f}$, this objective is equivalent to maximizing $\mu_{4,f} = \mu_4(\tau_f)$. In order to state the problem as minimization problem, the negative of $\mu_4(\tau_f)$ is chosen as one objective function. Moreover, τ_f is not fixed in unseeded crystallization because μ_3 depends on the supersaturation and cannot be expressed explicitly in terms of τ. Therefore, τ_f is determined during the optimization.

3.2 Pareto-Optimal Fronts for Multi-Objective Optimization Problems

For a multi-objective optimization problems, a Pareto-optimal front (PF) can show the trade-off between the objectives. A PF can be obtained using the weighted sum method[57]:

$$\phi(\tau_f) = \alpha\beta_1\phi_1(\tau_f) + (1-\alpha)\beta_2\phi_2(\tau_f) = \alpha\beta_1\phi_{1,f} + (1-\alpha)\beta_2\phi_{2,f} \tag{3.3}$$

where $\alpha \in [0,1]$, ϕ_1 and ϕ_2 are single objectives. Scaling factors β_1, β_2 are required because the two objectives usually have very different magnitude. The PF consists of a set of optimal solutions: each value of α corresponds to a point on the PF determined by solving the optimization problem. Optimal solutions with $\alpha = 0$ and $\alpha = 1$ give the endpoints of the PF, which are $(\phi_{1,f,max}, \phi_{2,f,min})$ and $(\phi_{1,f,min}, \phi_{2,f,max})$, respectively. The subscript min (or max) indicates the minimum (or maximum) value of the objective on the PF. In order to find the knee point, which can be considered to represent the best trade-off between objectives on the PF, normalized objective functions are defined as:

$$\phi_{1,f}'' = \frac{\phi_{1,f} - \phi_{1,f,min}}{\phi_{1,f,max} - \phi_{1,f,min}} \tag{3.4}$$

$$\phi_{2,f}'' = \frac{\phi_{2,f} - \phi_{2,f,min}}{\phi_{2,f,max} - \phi_{2,f,min}} \tag{3.5}$$

After normalization, the endpoints of the PF become $(1,0)$ and $(0,1)$. On the $\phi_{1,f}''$-$\phi_{2,f}''$ plane, the distance D from the origin to a given point is

$$D = \sqrt{\left(\phi_{1,f}''\right)^2 + \left(\phi_{2,f}''\right)^2} \tag{3.6}$$

The knee point is defined as the point on the PF for which D is minimized[58]. After finding the knee point on $\phi_{1,f}''$-$\phi_{2,f}''$ plane, the corresponding point on the $\phi_{1,f}$-$\phi_{2,f}$ plane can be determined. Figure 3.1 shows the Pareto-optimal fronts before and after the normalization.
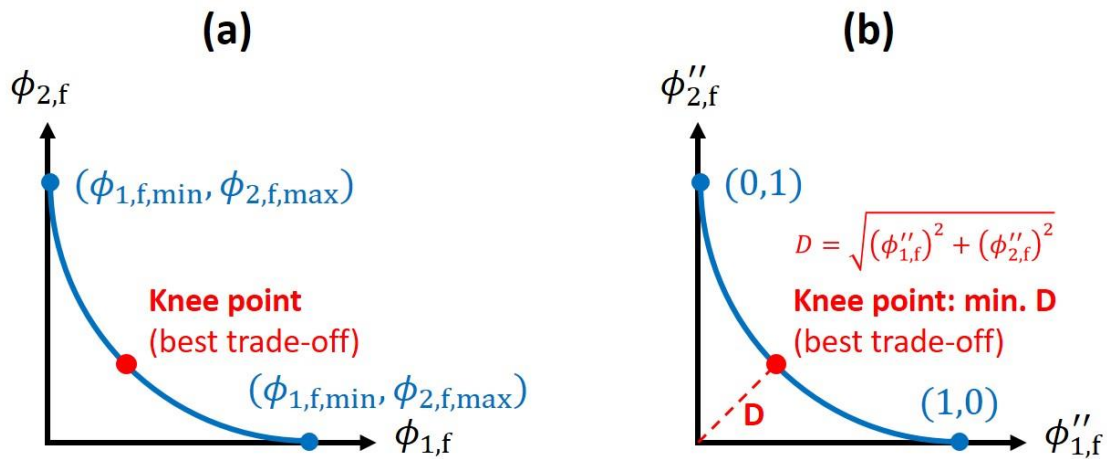

Figure 3.1. Pareto-optimal fronts: (a) before normalization, (b) after normalization.

By applying the weighted sum method[57], the objective function in each case can be written.

3.2.1 Case 1: Seeded Crystallization

In seeded crystallization, $\mu_{0,n,f} = \mu_{0,n}(\tau_f)$ and $\mu_{3,n,f} = \mu_{3,n}(\tau_f)$ are selected as the objectives to be minimized. Therefore, the objective function can be written as

$$\phi(\tau_f) = \alpha\beta_1\mu_{3,n}(\tau_f) + (1-\alpha)\beta_2\mu_{0,n}(\tau_f) = \alpha\beta_1\mu_{3,n,f} + (1-\alpha)\beta_2\mu_{0,n,f} \qquad (3.7)$$

3.2.2 Case 2: Unseeded Crystallization

In unseeded case, $-\text{WMS}_f = -\text{WMS}(\tau_f)$ and $\mu_{0,f} = \mu_0(\tau_f)$ are selected as the objectives to be minimized. Again the weighted sum method is applied [57]:

$$\phi(\tau_f) = \alpha\beta_1(-\text{WMS}_f) + (1-\alpha)\beta_2\mu_{0,f} \qquad (3.8)$$

3.3 Solutions to Optimization Problems

In this work, PMP is applied to provide necessary conditions for optimality (NCO) [37; 38], and all computations are performed in Matlab R2022a. Expressions for each of the optimization problems are first restated in terms of the state variables $\boldsymbol{x}$, and then be reformulated in terms of the Hamiltonian H with necessary conditions determined using PMP.

3.3.1 Case 1: Seeded Crystallization

In seeded crystallization, $\mu_{3,n}$ should be calculated because it is included in the mass balance and is one of the objectives to be minimized. Therefore, state variables x are defined as:

$$x_1 = \mu_{3,n}, x_2 = \mu_{2,n}, x_3 = \mu_{1,n}, x_4 = \mu_{0,n}, x_5 = t \tag{3.9}$$

Eq (3.1) can be expressed in terms of x, which is related to μ and t:

$$
\begin{aligned}
\min_{u(\tau)} \quad & \phi\big(x(\tau_\mathrm{f})\big) \\
\text{s.t.} \quad & \frac{dx}{d\tau} = F(x, u, \tau), x(0) = x_\mathrm{ini} \\
& \epsilon\big(x(\tau_\mathrm{f})\big) \leq 0 \\
& u(\tau) \in [u_\mathrm{lb}, \infty)
\end{aligned}
\tag{3.10}
$$

where u is the control input, which is defined as $u(\tau) = \frac{1}{G(\tau)}$ with a lower bound u_lb. x_ini is the initial condition of the state variables, and ϵ is a vector of terminal constraints. In this case, ϵ includes only one element, which is the batch time constraint, and ϵ can be expressed as $\epsilon = \big[x_5 - t_{\mathrm{f,c}}\big]$.

Application of PMP permits the reformulation of Eq 3.10 in terms of the Hamiltonian H with the corresponding necessary conditions:

$$\min_{\boldsymbol{u}(\tau)\in[u_{\mathrm{lb}},\infty)} H(\boldsymbol{x}, u, \boldsymbol{\psi}, \tau) = \boldsymbol{\psi}^{\mathrm{T}} \boldsymbol{F}(\boldsymbol{x}, u, \tau)$$

$$\mathrm{s.\,t.} \quad \frac{d\boldsymbol{x}}{d\tau} = \boldsymbol{F}(\boldsymbol{x}, u, \tau), \boldsymbol{x}(0) = \boldsymbol{x}_{\mathrm{ini}}$$

$$\frac{d\boldsymbol{\psi}}{d\tau} = -\frac{\partial H}{\partial \boldsymbol{x}}$$

$$\boldsymbol{\psi}^{\mathrm{T}}(\tau_{\mathrm{f}}) = \left[\left(\frac{\partial \phi}{\partial \boldsymbol{x}} \right) + \boldsymbol{v}^{\mathrm{T}} \left(\frac{\partial \boldsymbol{\epsilon}}{\partial \boldsymbol{x}} \right) \right] \Big|_{\tau_{\mathrm{f}}} \qquad (3.11)$$

$$\boldsymbol{v}^{\mathrm{T}} \boldsymbol{\epsilon} = 0$$

where $\boldsymbol{\psi}$ is a vector of costate variables with boundary conditions $\boldsymbol{\psi}(\tau_{\mathrm{f}})$, $\boldsymbol{v}$ is a vector

of Lagrange multipliers for terminal constraints, and superscript T represents the

transpose of a vector. $\boldsymbol{v}$ is non-negative when the terminal constraint is active and zero

otherwise. In this work, terminal constraints are assumed to be active.

From Eq 2.12, Eq 2.13, and the definition of state variables (Eq 3.9), differential

equations for each state can be derived:

$$\frac{dx_1}{d\tau} = 3x_2, \frac{dx_2}{d\tau} = 2x_3, \frac{dx_3}{d\tau} = x_4,$$

$$\frac{dx_4}{d\tau} = \frac{B}{G} \left(x_1 + \mu_{3,\mathrm{s}}(\tau), u(\tau) \right), \frac{dx_5}{d\tau} = u(\tau) \qquad (3.12)$$

where B is the nucleation rate, which is the sum of B_1 and B_2.

With the definition of the control input u and the expression for the growth rate G

(Eq 2.28), supersaturation S can be written in terms of u

$$S = 1 + (k_g u)^{\frac{-1}{g}} \qquad (3.13)$$

22
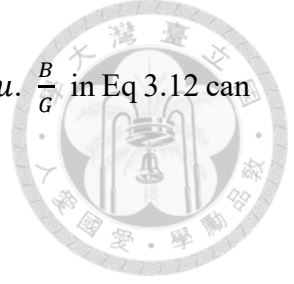
Nucleation rates B_1 and B_2 can also be expressed in terms of u. $\frac{B}{G}$ in Eq 3.12 can

then be written as

$$\frac{B}{G}(x_1 + \mu_{3,s}, u) =$$

$$u\left(k_{b1} \exp\left(\frac{-A}{\left(\ln\left(1 + (k_g u)^{\frac{-1}{g}}\right)\right)^2}\right) + k_{b2}(k_g u)^{\frac{-b}{g}}(x_1 + \mu_{3,s})^d\right) \qquad (3.14)$$

From Eq 3.11 and Eq 3.12, the Hamiltonian H can be written as

$$H(\boldsymbol{x}, u, \boldsymbol{\psi}, \tau) = 3\psi_1 x_2 + 2\psi_2 x_3 + \psi_3 x_4 + \psi_4 \frac{B}{G}\left(x_1 + \mu_{3,s}(\tau), u(\tau)\right) + \psi_5 u \qquad (3.15)$$

To simplify the calculations, Hofmann and Raisch[39] proposed that the nucleated

third moment $\mu_{3,n} = x_1$ in $H(\boldsymbol{x}, u, \boldsymbol{\psi}, \tau)$ can be neglected because nucleated moments

$\mu_{i,n}$ should be much smaller than the seed-grown moments $\mu_{i,s}$. This is reasonable

because the purpose of seeds is to absorb the supersaturation and suppress nucleation. It

is hoped that at the end of the batch that most of the precipitated mass has accrued to the

seeds and only a small portion to the nucleated crystals. When making this simplification,

it is important to check after optimization that the nucleated mass is indeed small

compared to the seed grown mass. This verification is performed for the case study system

in Section 4.2. Based on this assumption, $x_1 + \mu_{3,s}$ in Eq 3.14 can be replaced by $\mu_{3,s}$,

and Eq 3.15 can then be written as
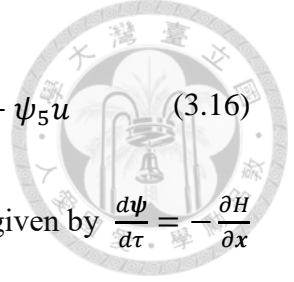
$$H(\boldsymbol{x}, u, \boldsymbol{\psi}, \tau) = 3\psi_1 x_2 + 2\psi_2 x_3 + \psi_3 x_4 + \psi_4 \frac{B}{G}\left(\mu_{3,s}(\tau), u(\tau)\right) + \psi_5 u \qquad (3.16)$$

The following are the differential equations for the costate variables given by $\frac{d\boldsymbol{\psi}}{d\tau} = -\frac{\partial H}{\partial \boldsymbol{x}}$

in Eq 3.11:

$$\frac{d\psi_1}{d\tau} = 0, \frac{d\psi_2}{d\tau} = -3\psi_1, \frac{d\psi_3}{d\tau} = -2\psi_2,$$
$$\frac{d\psi_4}{d\tau} = -\psi_3, \frac{d\psi_5}{d\tau} = 0 \qquad (3.17)$$

with boundary conditions given by $\boldsymbol{\psi}^{\mathrm{T}}(\tau_{\mathrm{f}}) = \left[\left(\frac{\partial \phi}{\partial \boldsymbol{x}}\right) + \boldsymbol{v}^{\mathrm{T}}\left(\frac{\partial \boldsymbol{\epsilon}}{\partial \boldsymbol{x}}\right)\right]\Big|_{\tau_{\mathrm{f}}}$. The first term

depends on the objective function, and the second term is given by:
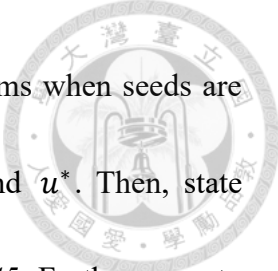
$$\boldsymbol{v}^{\mathrm{T}}\left(\frac{\partial \boldsymbol{\epsilon}}{\partial \boldsymbol{x}}\right) = [0,0,0,0,v_5] \qquad (3.18)$$

where v_5 is a non-negative constant. With an initial guess for v_5, $\boldsymbol{\psi}$ can be solved by

analytical integration.

In addition, the optimal control input u^* at each instant of τ must satisfy the

following NCO:

$$u^* = \underset{\boldsymbol{u}(\tau)\in[u_{\mathrm{lb}},\infty)}{\mathrm{argmin}} H(\boldsymbol{x}, u, \boldsymbol{\psi}, \tau) = \underset{\boldsymbol{u}(\tau)\in[u_{\mathrm{lb}},\infty)}{\mathrm{argmin}} \psi_4 \frac{B}{G}\left(\mu_{3,s}(\tau), u(\tau)\right) + \psi_5 u \qquad (3.19)$$

However, it is difficult to obtain an analytical solution because of the complicated

expression for $\frac{B}{G}$. In this work, the function *fminbnd* in Matlab is used to find u^*

numerically.

24

The following is the procedure for solving optimization problems when seeds are present. First, make an initial guess of ν_5, solve $\boldsymbol{\psi}$, and then find u^*. Then, state variables $\boldsymbol{x}$ can be determined by integration using the solver *ode45*. Furthermore, to satisfy the batch time constraint, the value of ν_5 is determined by iteration using the function *fzero* until $x_5(\tau_f) = t_{f,c}$. After iteration, ν_5 is determined and product properties can be obtained ($\mu_{3,n}(\tau_f) = x_1(\tau_f)$, $\mu_{0,n}(\tau_f) = x_4(\tau_f)$). Finally, it is critical to check whether $\mu_{3,s}$ is indeed much larger than $\mu_{3,n}$ because this assumption is used in Eq 3.16. Figure 3.2 shows the flowchart of the optimization procedure for seeded crystallization processes.

25
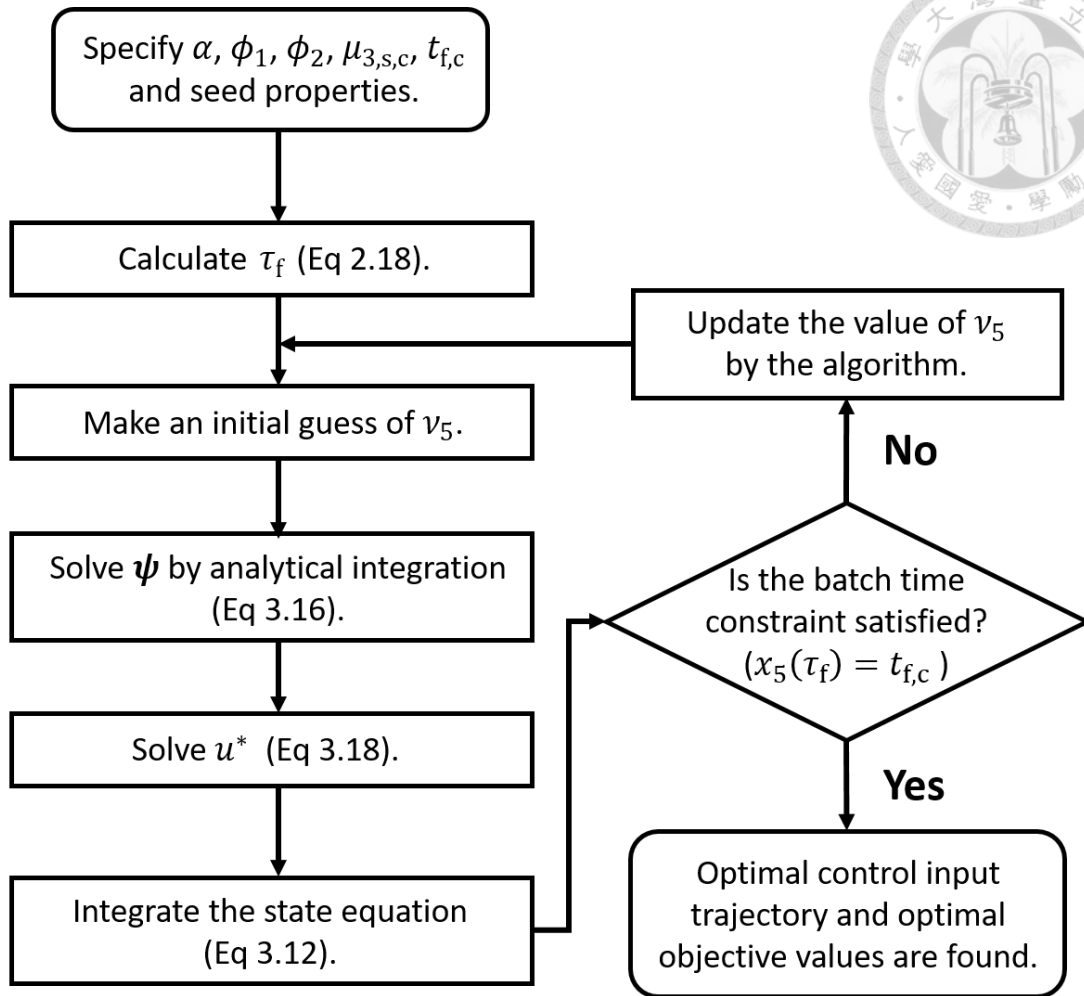
Figure 3.2. Flowchart of solving optimization problems for seeded case.

3.3.2 Case 2: Unseeded Crystallization

In unseeded crystallization, μ_4 should also be calculated because its value is needed to calculate the objective WMS=$(\frac{\mu_4}{\mu_3})$. Thus, the definition of x is slightly different than in the seeded case:

$$x_1 = \mu_4, x_2 = \mu_3, x_3 = \mu_2, x_4 = \mu_1, x_5 = \mu_0, x_6 = t \tag{3.20}$$

Eq 3.2 can then be restated as

$$
\min_{u(\tau),\tau_{\mathrm{f}}} \quad \phi\big(\boldsymbol{x}(\tau_{\mathrm{f}})\big)
$$

$$
\text{s.t.} \quad \frac{d\boldsymbol{x}}{d\tau} = \boldsymbol{F}(\boldsymbol{x},u,\tau), \boldsymbol{x}(0) = \boldsymbol{x}_{\mathrm{ini}}
$$

$$
\boldsymbol{\epsilon}\big(\boldsymbol{x}(\tau_{\mathrm{f}})\big) \leq \mathbf{0}
$$

$$
u(\tau) \in [u_{\mathrm{lb}}, \infty) \tag{3.21}
$$

In this case, τ_{f} has to be determined, and the final constraint on the product should be included in $\boldsymbol{\epsilon}$. Therefore, $\boldsymbol{\epsilon}$ can be expressed as $\boldsymbol{\epsilon} = \big[x_2 - \mu_{3,\mathrm{c}}, x_6 - t_{\mathrm{f,c}}\big]^{\mathrm{T}}$ representing the production rate constraint and the batch time constraint.

Next, Eq 3.21 can be reformulated by applying PMP:

$$
\min_{\boldsymbol{u}(\tau)\in[u_{\mathrm{lb}},\infty),\tau_{\mathrm{f}}} \quad H(\boldsymbol{x},u,\boldsymbol{\psi},\tau) = \boldsymbol{\psi}^{\mathrm{T}}\boldsymbol{F}(\boldsymbol{x},u,\tau)
$$

$$
\text{s.t.} \quad \frac{d\boldsymbol{x}}{d\tau} = \boldsymbol{F}(\boldsymbol{x},u,\tau), \boldsymbol{x}(0) = \boldsymbol{x}_{\mathrm{ini}}
$$

$$
\frac{d\boldsymbol{\psi}}{d\tau} = -\frac{\partial H}{\partial \boldsymbol{x}} \tag{3.22}
$$

$$
\boldsymbol{\psi}^{\mathrm{T}}(\tau_{\mathrm{f}}) = \left[\left(\frac{\partial \phi}{\partial \boldsymbol{x}}\right) + \boldsymbol{v}^{\mathrm{T}}\left(\frac{\partial \boldsymbol{\epsilon}}{\partial \boldsymbol{x}}\right)\right]\Big|_{\tau_{\mathrm{f}}}
$$

$$
\boldsymbol{v}^{\mathrm{T}}\boldsymbol{\epsilon} = 0
$$

Then the differential equations for state variables can be derived:

$$
\frac{dx_1}{d\tau} = 4x_2, \frac{dx_2}{d\tau} = 3x_3, \frac{dx_3}{d\tau} = 2x_4,
$$

$$
\frac{dx_4}{d\tau} = x_5, \frac{dx_5}{d\tau} = \frac{B}{G}\big(x_2, u(\tau)\big), \frac{dx_6}{d\tau} = u(\tau) \tag{3.23}
$$

In this case, $\frac{B}{G}\big(x_2, u(\tau)\big)$ cannot be simplified by neglecting the nucleated mass because all crystals are nucleus-grown.

27
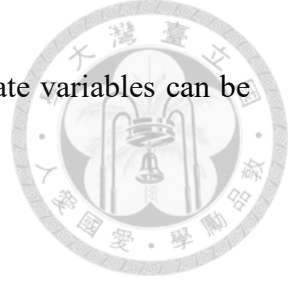
The Hamiltonian H, and the differential equations for the costate variables can be written as

$$H(\boldsymbol{x}, u, \boldsymbol{\psi}, \tau) = 4\psi_1 x_2 + 3\psi_2 x_3 + 2\psi_3 x_4 + \psi_4 x_5 + \psi_5 \frac{B}{G}\big(x_2, u(\tau)\big) + \psi_6 u \qquad (3.24)$$

$$\frac{d\psi_1}{d\tau} = 0, \frac{d\psi_2}{d\tau} = -4\psi_1 - \frac{\partial\left(\dfrac{B}{G}\big(x_2, u(\tau)\big)\right)}{\partial x_2}, \frac{d\psi_3}{d\tau} = -3\psi_2,$$
$$\frac{d\psi_4}{d\tau} = -2\psi_3, \frac{d\psi_5}{d\tau} = -\psi_4, \frac{d\psi_6}{d\tau} = 0 \qquad (3.25)$$

However, costate variables $\boldsymbol{\psi}$ cannot be integrated directly with the boundary conditions given by $\boldsymbol{\psi}^{\mathrm{T}}(\tau_{\mathrm{f}}) = \left[\left(\dfrac{\partial\phi}{\partial x}\right) + \boldsymbol{\nu}^{\mathrm{T}}\left(\dfrac{\partial\epsilon}{\partial x}\right)\right]\Big|_{\tau_{\mathrm{f}}}$ because both x_2 and $u(\tau)$ appear in the differential equations. In this case, $\boldsymbol{\nu}^{\mathrm{T}}\left(\dfrac{\partial\epsilon}{\partial x}\right)$ is given by $\boldsymbol{\nu}^{\mathrm{T}}\left(\dfrac{\partial\epsilon}{\partial x}\right) = [0, \nu_2, 0, 0, 0, \nu_6]$, where ν_2 and ν_6 are constants.

To obtain the optimal control input u^*, the following NCO must be satisfied:

$$\frac{\partial H}{\partial u}\bigg|_{u^*} = \psi_5 \frac{\partial\left(\dfrac{B}{G}\right)}{\partial u}\bigg|_{u^*} + \psi_6 = 0 \qquad (3.26)$$

The trajectory of $u(\tau)$ consists of two parts: an unconstrained arc ($u \neq u_{\mathrm{lb}}$) and a constrained arc ($u = u_{\mathrm{lb}}$). The switching time denoted as τ_s means the switching instant between these arcs (see Figure 3.3). Because the trajectory of $u(\tau)$ is continuous, the NCO (Eq 3.26) should also be satisfied at the switching time if τ_s exists.
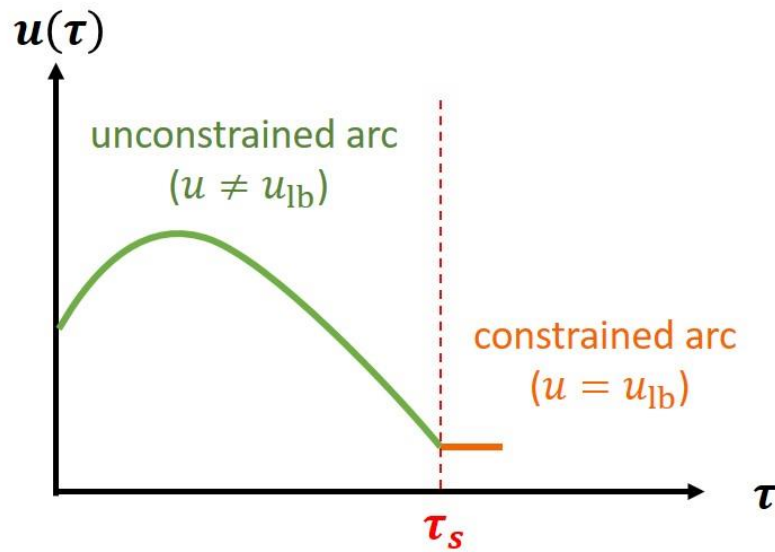
28

Figure 3.3. Constrained arc, unconstrained arc, and the switching time.

In addition, for an optimization problem with a free terminal time (τ_f), an additional condition called the transversality condition must be satisfied [38; 52; 59]:

$$H(\tau_\text{f}) = \left(\boldsymbol{\psi}^\text{T}\boldsymbol{F}(\boldsymbol{x}, u, \tau)\right)\Big|_{\tau_\text{f}} = 0 \tag{3.27}$$

This case is more complicated because $\boldsymbol{\psi}$ cannot be integrated directly. In this work, the gradient method is applied to solve this boundary value problem numerically [52-54]. The following is the procedure for applying the gradient method.

At first, the constraint on the control input is assumed to be inactive, i.e. τ_s does not exist. Then, $u(\tau)$ is discretized into N points and an initial guess for all $N + 3$ decision variables is made: $u(\tau_1),\ u(\tau_2), ...,\ u(\tau_N),\ v_2,\ v_6,\ \tau_\text{f}$. With N discretization points, $u(\tau)$ at any instant is obtained using the piecewise cubic interpolation function *pchip* in Matlab.

29
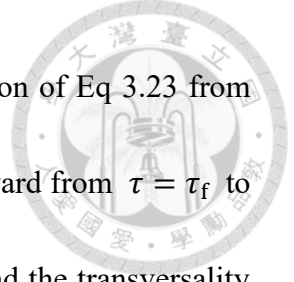
After determining $u(\tau)$, $\boldsymbol{x}$ can be solved by forward integration of Eq 3.23 from $\tau = 0$ to $\tau = \tau_f$, and $\boldsymbol{\psi}$ can be found by integrating Eq 3.25 backward from $\tau = \tau_f$ to $\tau = 0$. Next, in order to satisfy the NCO, the terminal constraints and the transversality condition, a vector $\boldsymbol{R}$ is constructed with $N + 3$ elements:

$$R_i = \psi_5(\tau_i) \left. \frac{\partial \left(\frac{B}{G}\right)}{\partial u} \right|_{u(\tau_i)} + \psi_6(\tau_i), i = 1, \dots, N \tag{3.28}$$

$$R_{N+1} = x_2(\tau_f) - \mu_{3,c} \tag{3.29}$$

$$R_{N+2} = x_6(\tau_f) - t_{f,c} \tag{3.30}$$

$$R_{N+3} = \left. \left(\boldsymbol{\psi}^T \boldsymbol{F}(\boldsymbol{x}, u, \tau)\right) \right|_{\tau_f} \tag{3.31}$$

where R_i $(i = 1, \dots, N)$ are the NCO, R_{N+1} and R_{N+2} are terminal constraints, and R_{N+3} is the transversality condition. All of these conditions will be satisfied if each element in $\boldsymbol{R}$ is equal to zero.

In this work, the 2-norm of $\boldsymbol{R}$ $(\|\boldsymbol{R}\|_2)$ is selected as the function to be minimized. The nonlinear least-squares solver *lsqnonlin* in Matlab is used to perform the optimization: updating the decision variables and integrating $\boldsymbol{x}$ and $\boldsymbol{\psi}$ at each iteration until $\|\boldsymbol{R}\|_2$ is lower than the termination tolerance.

In order to determine whether τ_s exists, the lower bound on the control input is first set lower than its constraint in *lsqnonlin*. Then, the optimization results are checked to determine whether the constraint on the control input is active during the batch. If it is

30

active, τ_s should be included in the decision variables, and an additional NCO should be added in the residual vector $\boldsymbol{R}$:

$$R_{N+4} = \psi_5(\tau_s) \left. \frac{\partial \left(\frac{B}{G} \right)}{\partial u} \right|_{u(\tau_s)} + \psi_6(\tau_s) \tag{3.32}$$

The optimization is performed again. Finally, the trajectory of optimal control input can be determined, and product properties ($\mu_{0,f}$ and WMS_f) can also be obtained. Figure 3.4 shows the procedure for applying the gradient method to solve the optimization problems for unseeded crystallization processes.
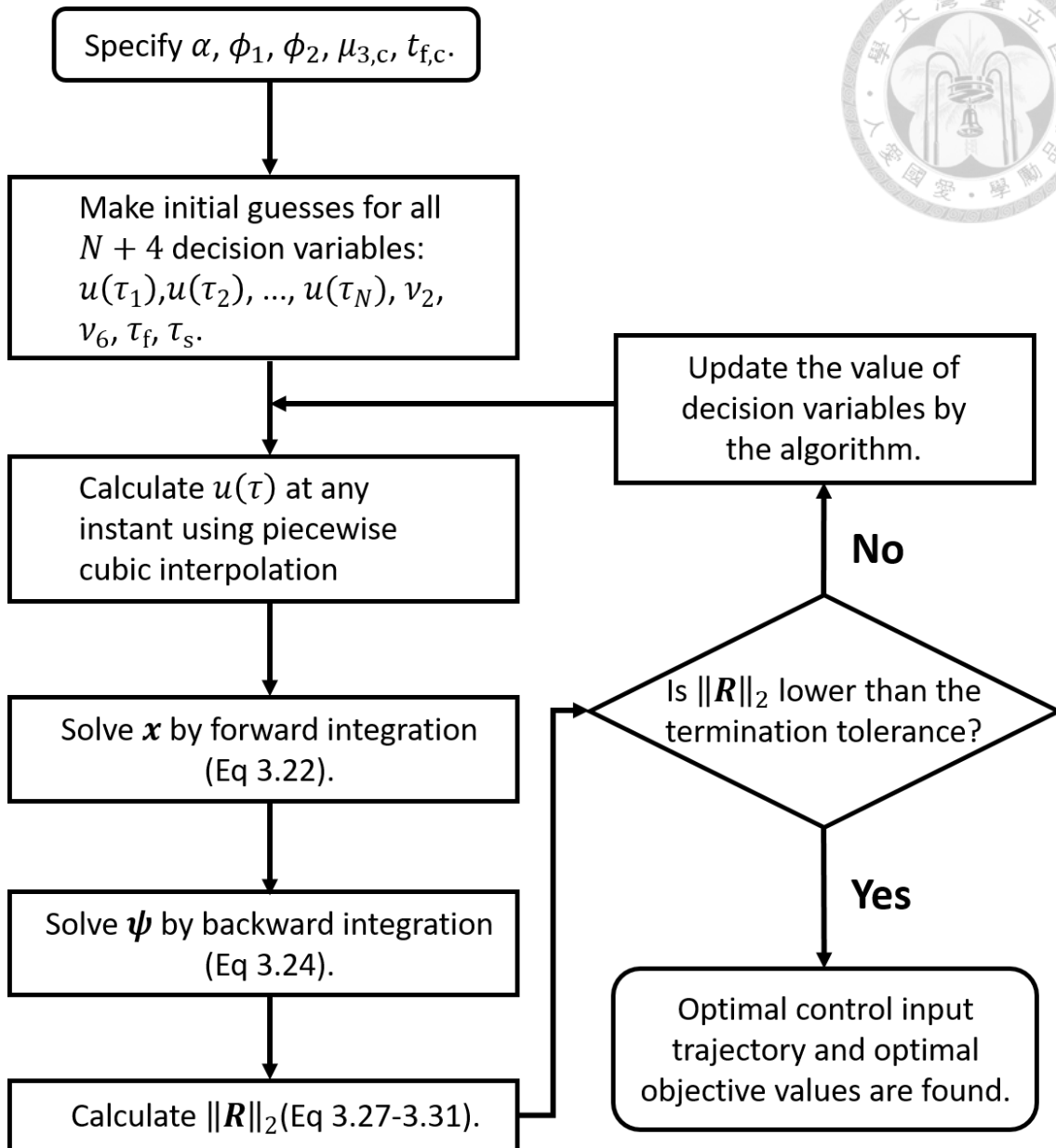
Figure 3.4. Flowchart of solving optimization problems for unseeded case.

Chapter 4 Case Study

In this chapter, a case study is used to illustrate the proposed framework in this work. In Section 4.1, the system is briefly introduced, and the parameters for the system are listed. Optimization results for each case are presented and discussed in Section 4.2.

4.1   Parameters for the System

The crystallization of ampicillin from water is considered in this work. Crystallization kinetics are adapted from Encarnación-Gómez et al.[60], whose experiments were based on pH-induced supersaturation. 1 M HCl is added into the system to gradually change the pH value (from about 7.8 to about 6.5), which affects the solubility. Table 4.1 shows the parameters used in the case study, and the crystallization kinetics are given in Eqs 2.28-2.32. Figure 4.1 shows primary and secondary nucleation rates as a function of supersaturation for $\mu_3 = 100$ cm3. It is shown in the figure that primary nucleation is dominant when $S > 1.3$. Therefore, it is expected that primary nucleation might dominate in this case. Although this is not common in industrial processes[61], the proposed method in this work can be applied to any other crystallization system with deterministic expressions for crystal growth rate and primary and secondary nucleation rates, even if secondary nucleation is dominant.
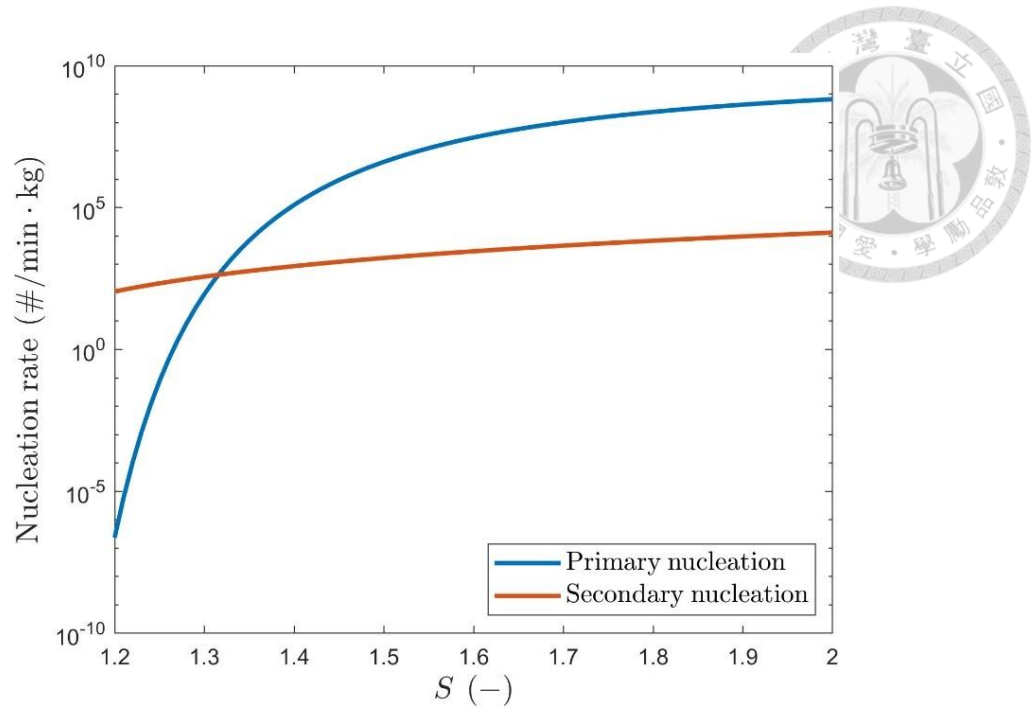
Figure 4.1. The relation between nucleation rates and the supersaturation.

For seeded crystallization, assume the seed CSD $f_s(L, 0)$ is given by

$$f_s(L, 0) = N_0 \cdot \delta(L - L_0) \tag{4.1}$$

where N_0 and L_0 are the number and size of the seeds, respectively. From Eqs 2.3 and 4.1, the ith moment of seed crystals $\mu_{i0,s}$ can be calculated. In addition, $\mu_{3,s,c}$ is the final constraint on $\mu_{3,s}$, which is set by making $\mu_{3,s,c} - \mu_{3,s,0}$ equal to 100.00 cm³/kg.

34

Table 4.1. Parameters for the system[60]

Parameter	Description	Value	Unit
k_g	Growth rate constant	4.50	μm/min
g	Growth rate exponent	2.32	-
k_{b1}	Primary nucleation rate constant	9.27×10^9	#/(min·kg)
A	Primary nucleation constant	1.27	-
k_{b2}	Secondary nucleation rate constant	1.32×10^2	#/(min·kg)/(cm^3/kg)^d
b	Secondary nucleation rate exponent	2.97	-
d	Nucleation rate exponent of μ_3	1.00	-
$\mu_{3,s,0}$	Initial $\mu_{3,s}$ in seeded case	8.10	cm^3/kg
$\mu_{3,s,c}$	Final constraint on $\mu_{3,s}$ in seeded case	108.10	cm^3/kg
$\mu_{3,c}$	Final constraint on μ_3 in unseeded case	200.00	cm^3/kg
$t_{f,c}$	Final batch time constraint	200.00	min
S_{ub}	Upper bound of the supersaturation	1.64	-
N_0	Number of the seed	2.00×10^7	#/kg
L_0	Size of the seed	74.00	μm
ρ	Crystal density	1.50×10^3	kg/ m^3
k_V	Volume shape factor	0.03	-
pH$_{ini}$	Initial pH value	7.60	-
C_{ini}	Initial concentration	19.95	g/kg

4.2 Results and Discussion

4.2.1 Case 1: Seeded Crystallization

In seeded case, there is a final constraint on $\mu_{3,s}$, so τ_f can be determined directly

from Eq 2.18 based on the production rate constraint $\mu_{3,s}(\tau_f) = \mu_{3,s,c}$. In this work,

$\mu_{3,n,f} = \mu_{3,n}(\tau_f)$ and $\mu_{0,n,f} = \mu_{0,n}(\tau_f)$ are selected as the objectives to be minimized.

Figure 4.2(a) shows the PF on $\mu_{3,n,f}$-$\mu_{0,n,f}$ plane. Point A is the point minimizing $\mu_{3,n,f}$,

point B is the knee point, and point C is the point minimizing $\mu_{0,n,f}$. The values of both
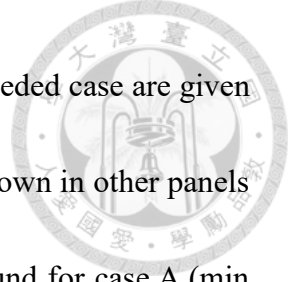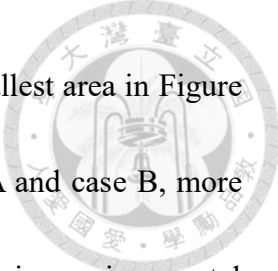
objective functions at these three points on the Pareto front for the seeded case are given

in Table 4.2. The optimization results of these three cases are also shown in other panels

of Figure 4.2. In Figure 4.2(b), a late growth operating policy is found for case A (min

$\mu_{3,\mathrm{n,f}}$) and case B (knee point). This result is consistent with the previous work: objectives

involving higher nucleated moments would lead to late growth operating policies[7].

However, the supersaturation remains almost constant for case C (min $\mu_{0,\mathrm{n,f}}$). The reason

is that the primary nucleation rate (Figure 4.2(c)) is always much higher than secondary

nucleation rate (Figure 4.2(d)). In this case, an approximation of the optimal control input

for case C can be obtained by solving Eq 3.19 with $\psi_4 = 1$, $\psi_5 = \nu_5$, and $B_1 \gg B_2$. Eq

3.19 then becomes

$$u^* = \underset{\boldsymbol{u}(\tau)\in[u_{\mathrm{lb}},\infty)}{\mathrm{argmin}} \; (B_1 + B_2)u + \nu_5 u \approx \underset{\boldsymbol{u}(\tau)\in[u_{\mathrm{lb}},\infty)}{\mathrm{argmin}} \; B_1 u + \nu_5 u \tag{4.2}$$

Since B_1 depends only on u, and ν_5 is constant, u^* does not change with time,

resulting in an almost constant supersaturation.

In addition, population density functions (PDFs) $f_{\mathrm{n,f}}(L)$ and volume density

functions (VDFs) $L^3 f_{\mathrm{n,f}}(L)$ for the nucleated product can be calculated using Eq 2.27,

and are shown in Figure 4.2(e) and Figure 4.2(f), respectively. Based on the definition of

the moments of the CSD, $\mu_{0,\mathrm{n,f}}$ and $\mu_{3,\mathrm{n,f}}$ are the area under the PDF curve and VDF

curve, respectively. In case A, the objective is to minimize $\mu_{3,\mathrm{n,f}}$, so the area under the

36

curve in Figure 4.2(f) is the smallest. By contrast, case C has the smallest area in Figure 4.2(e). In addition, for a late growth operating policy, such as case A and case B, more nuclei are formed at the end of the batch, so the PDF decreases with increasing crystal size (see Figure 4.2(e)). Since these nuclei do not have enough time to grow, their size and volume are very small (see Figure 4.2(f)). Therefore, it is reasonable that a late growth operating policy is preferred for minimizing $\mu_{3,n,f}$. On the other hand, for a constant supersaturation operating policy, such as case C, nuclei are formed more uniformly in time. Although the number of nucleated crystals is smaller, the nuclei formed at the beginning of the batch grow large and achieve a large volume.

Panels (c) and (d) show that primary nucleation dominates over secondary nucleation throughout the batch for all three cases. This result follows inherently from the crystallization kinetics. In practice secondary nucleation could be neglected with almost no effect on the results. Secondary nucleation is included here in order to demonstrate that the algorithm can optimize crystallization processes where both primary and secondary nucleation occur.

Finally, it is necessary to verify the assumption made in the calculation. In order to simplify the expression of the Hamiltonian in Eq 3.15, $\mu_{3,n}$ is assumed to be much lower than $\mu_{3,s}$. Table 4.1 shows that the third moment of the seed-grown crystals increases from 8.10 cm^3/kg (seeding condition) to 108.10 cm^3/kg for every batch to satisfy the

37

production rate constraint. However, in case C (min $\mu_{0,n,f}$), for which $\mu_{3,n,f}$ is the

greatest of any point on the PF, the third moment of the nucleated product is only 4.06

cm^3/kg (see Table 4.2). Therefore, the nucleated product only accounts for 3.76% of the

total product crystal volume. Therefore, it is reasonable to assume that the nucleated mass

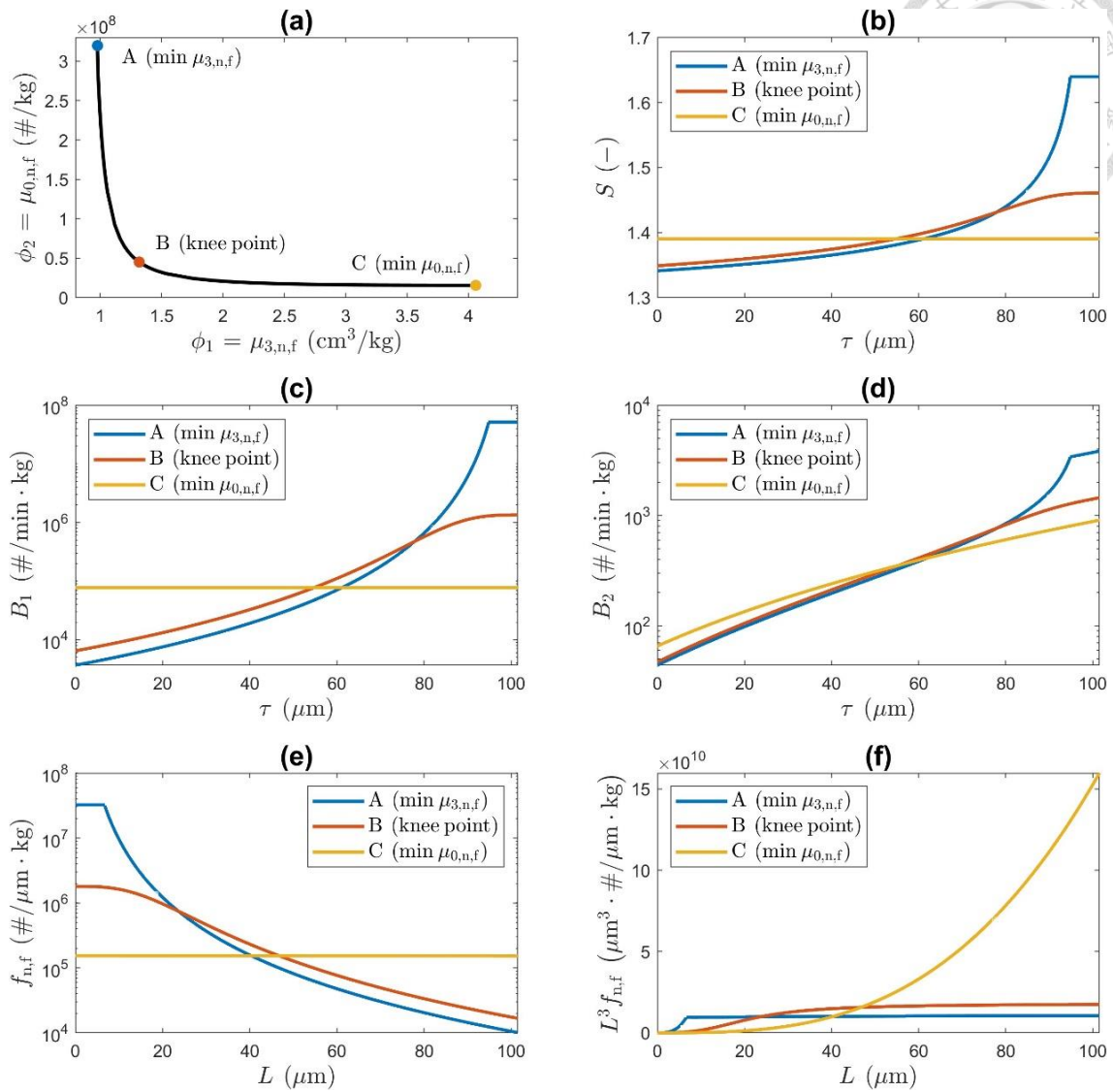can be neglected in the material balance.

38
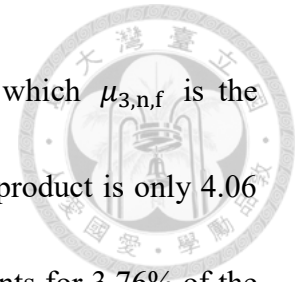
Figure 4.2. Results of seeded case: (a) Pareto-optimal front, (b) supersaturation

trajectories, (c) primary nucleation rate trajectories, (d) secondary nucleation rate

trajectories, (e) population density functions, (f) volume density functions.

Table 4.2. Values of objective functions for the seeded case

Point	$\mu_{3,n,f}$ (cm^3/kg)	$\mu_{0,n,f}$ (#/kg)
A (min $\mu_{3,n,f}$)	0.98	3.20×10^8
B (knee point)	1.32	4.51×10^7
C (min $\mu_{0,n,f}$)	4.06	1.56×10^7

In this case study, supersaturation is induced by lowering the pH of the solution by adding a strong acid (pH-induced supersaturation). The optimization procedure described in our work determines the optimal supersaturation trajectory during the batch. This can then be converted to a pH trajectory (indicating how the pH should change with time during the batch) using Eq 2.31, Eq 2.32, and experimental data for the solubility of ampicillin as a function of pH (see Figure 4.3) given by Encarnación-Gómez et al.[60]. Figure 4.3 shows the relationship between the solubility and the pH, but the data are only applicable when the pH value is in the range of 5.0 and 7.6.

Figure 4.4 shows the results of optimal control input profiles, supersaturation and pH, in the time domain. In practical case, the pH trajectory can be used to determine an acid flow rate trajectory (indicating how the flow rate of acid should change with time during the batch) using material balances and knowledge of acid-base chemistry. However, in this case, it might be difficult to control the pH value accurately because the optimal value at each instant is close to 7.
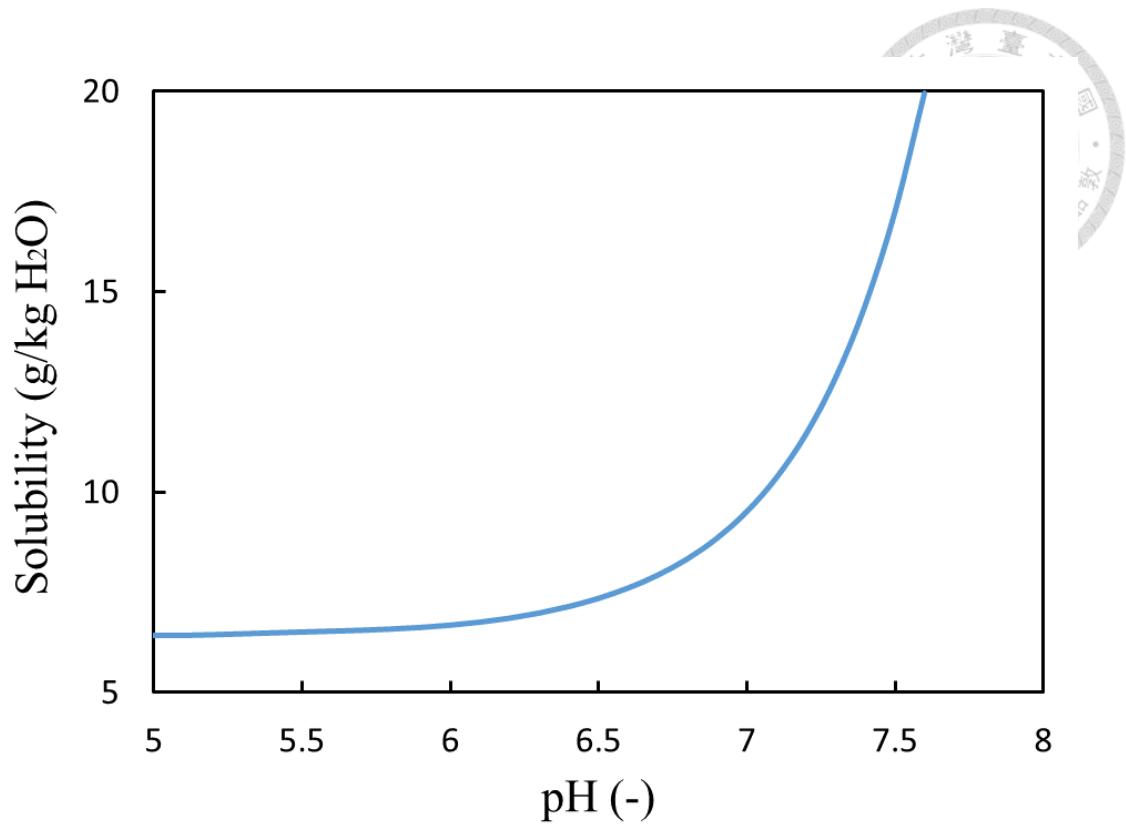
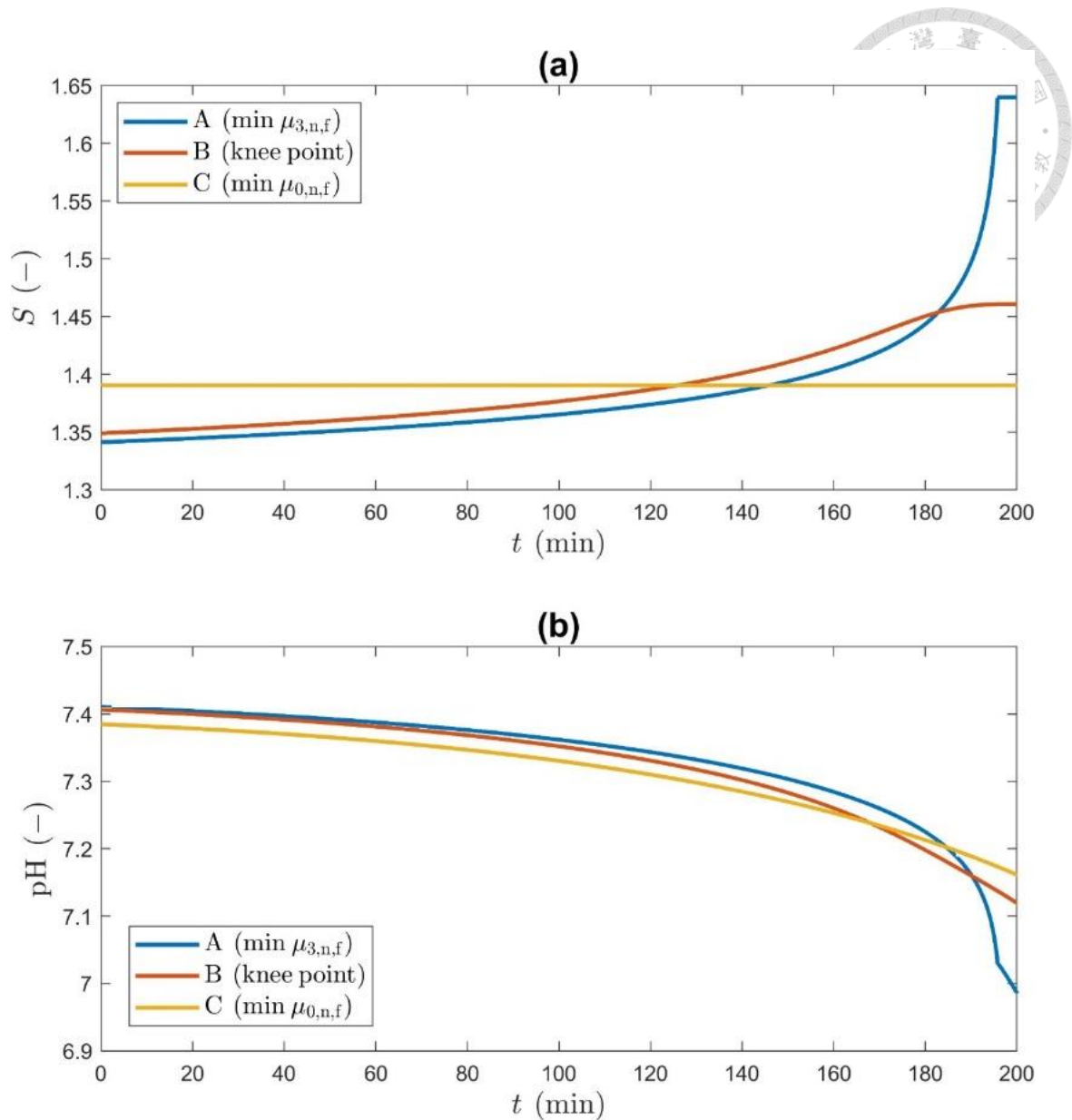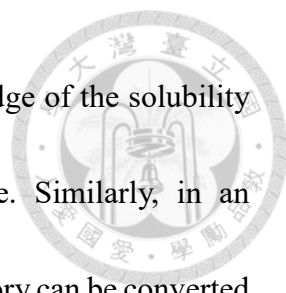Figure 4.3. Solubility data for ampicillin in water [60].

Figure 4.4. Results of optimal control input profiles in time domain in seeded case: (a)

supersaturation trajectories, (b) pH value trajectories.

In addition, the optimization method proposed in this work is not limited to pH-induced supersaturation. It is applicable regardless of the method by which supersaturation is induced. For example, in a cooling crystallization, the method would again produce the optimal supersaturation trajectory. This could then be converted to the

42

optimal temperature trajectory using a material balance and knowledge of the solubility of the substance being crystallized as a function of temperature. Similarly, in an evaporative crystallization process, the optimal superaturation trajectory can be converted to a trajectory indicating the rate at which solvent should be evaporated.

4.2.2 Case 2: Unseeded Crystallization

In this case, $-\text{WMS}_{\text{f}} = -\text{WMS}(\tau_{\text{f}})$ and $\mu_{0,\text{f}} = \mu_0(\tau_{\text{f}})$ are selected as the objectives to be minimized. Optimization of unseeded crystallization processes is more challenging. In order to apply a gradient method, it is necessary to determine first whether the growth rate constraint becomes active during the batch, i.e. whether a switching time τ_{s} exists in the supersaturation trajectory. After determining initial guesses for all decision variables, the nonlinear least-squares solver *lsqnonlin* in Matlab is used to minimize the 2-norm of the residuals vector ($\|\boldsymbol{R}\|_2$). However, the algorithm may terminate early because either the step size tolerance or the maximum number of iterations is reached. Therefore, it is critical to check whether the function value ($\|\boldsymbol{R}\|_2$) and the trajectory of optimal control input are reasonable after solving each problem. Ten points on the PF are solved individually, and the function *pchip* in Matlab is used for interpolation (see Figure 4.5(a)). Point A is the case maximizing WMS_{f}, point B is the point closest to the knee point, and point C is the case minimizing $\mu_{0,\text{f}}$. The values of

both objective functions at these three points on the Pareto front for the unseeded case are given in Table 4.3. The optimization results of these three cases are shown in Figure 4.5. Figure 4.5(b) shows that a late growth operating policy is preferred for case A (max WMS_f) , and that an early growth operating policy is preferred for case B (closest to the knee point) and case C (min $\mu_{0,f}$). In addition, results show that switching time τ_s exists in case A and case C, with values 149 μm and 1.44 μm respectively. In unseeded crystallization, τ_f is the decision variable used to satisfy the final constraint on μ_3. In this work, τ_f is largest in case A ($\tau_f = 149$ μm) and smallest in case C ($\tau_f = 123$ μm). The primary nucleation rate depends only on the supersaturation, so the trend in Figure 4.5(c) is similar to that in Figure 4.5(b). On the other hand, the secondary nucleation rate depends both on the supersaturation and μ_3 , but supersaturation dominates at the beginning of the batch because $\mu_3(0)$ is equal to 0. Since case C results in an early growth operating policy, the secondary nucleation rate is the highest in the beginning (see Figure 4.5(d)). However, the secondary nucleation rates of all three cases are very similar at the end of the batch because the constraint on μ_3 is the same for every case.

PDFs and VDFs for the product are calculated using Eq 2.21 and are shown in Figure 4.5(e) and Figure 4.5(f), respectively. In Case C, the objective is to minimize $\mu_{0,f}$ and the resulting optimal supersaturation trajectory is early growth. Therefore more nuclei are formed in the beginning. They have enough time to grow and account for larger share of

44

the product volume. In case A (max WMS_f), a late growth operating policy is preferred, so fewer nuclei are formed in the beginning compared to case C. With the same final constraint on μ_3, the areas under VDFs in each case should be the same (see Figure 4.5(f)). Therefore, τ_f should be larger in case A than in case C.

It can also be seen from Panel (f) that case A has a larger WMS than cases B and C. Since WMS_f is defined as $\frac{\mu_{4,f}}{\mu_{3,f}}$ and $\mu_{3,f}$ is the same in each case, WMS depends only on $\mu_{4,f}$, which is the area under the curve $L^4 f_{n,f}(L)$. Furthermore, the areas under VDFs $(L^3 f_{n,f}(L)$ versus $L)$ of all three cases are the same, and τ_f is larger in case A. Therefore, it can be expected that the area under the curve $L^4 f_{n,f}(L)$ is larger in case A, resulting in a lager value of $\mu_{4,f}$ and a larger WMS_f.
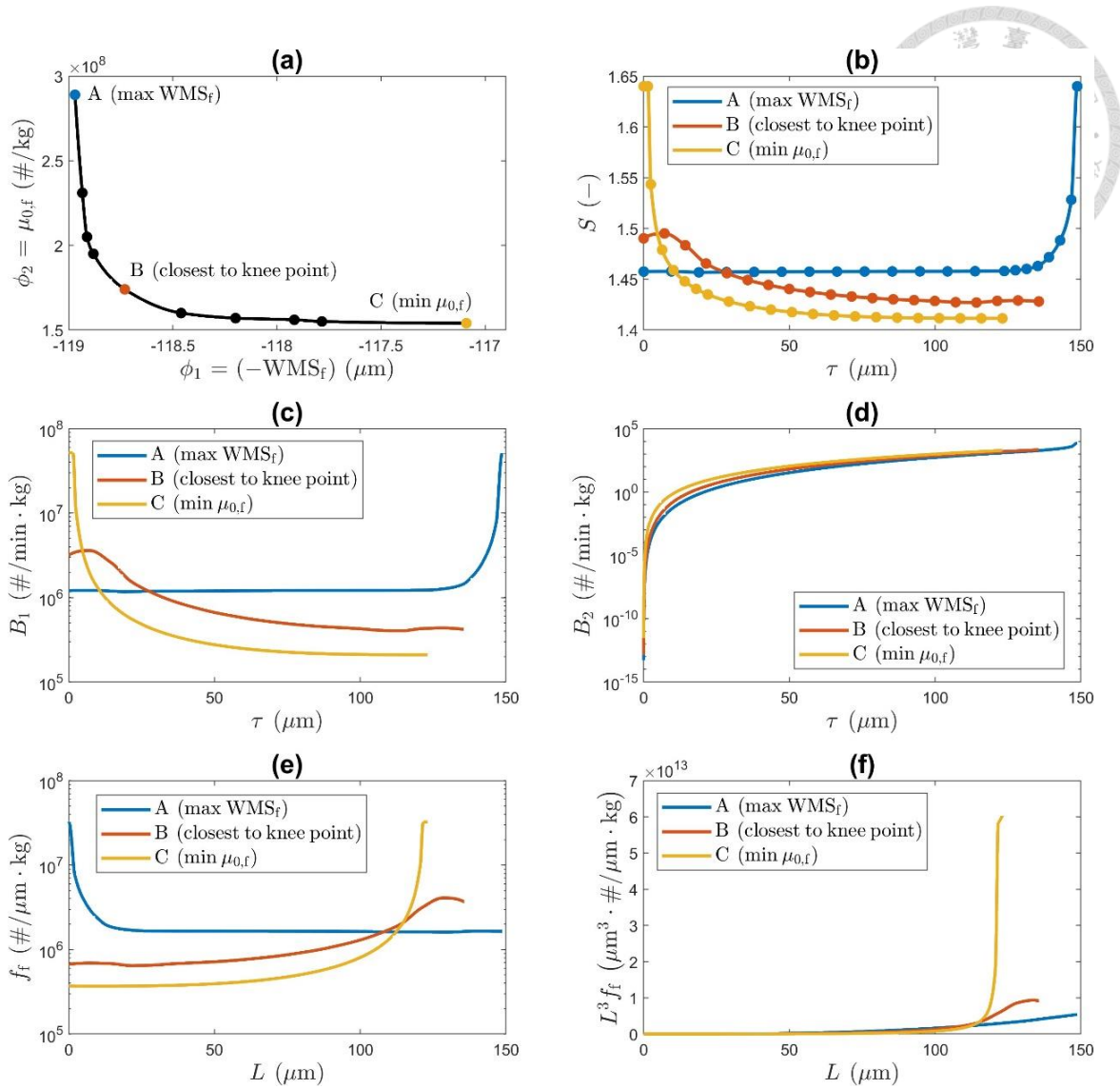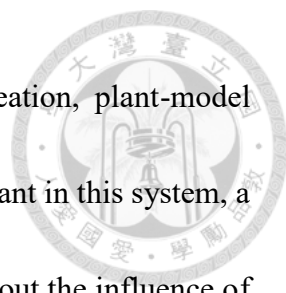
Figure 4.5. Results of unseeded case: (a) Pareto-optimal front, (b) supersaturation

trajectories, (c) primary nucleation rate trajectories, (d) secondary nucleation rate

trajectories, (e) population density functions, (f) volume density functions.

Table 4.3. Values of objective functions for the unseeded case

Point	WMS_f (μm)	$\mu_{0,f}$ (#/kg)
A (max WMS_f)	118.97	2.89×10^8
B (closest to knee point)	118.73	1.74×10^8
C (min $\mu_{0,f}$)	117.09	1.54×10^8

46

However, due to the complex and stochastic nature of nucleation, plant-model mismatch is a concern. Considering that primary nucleation is dominant in this system, a sensitivity analysis of primary nucleation rate is conducted to figure out the influence of the uncertainties. The primary nucleation rate constant k_{b1} is either increased or decreased by 10% compared to its original value, then the optimization is performed again. Figure 4.6 shows the results of sensitivity analysis for case A (max WMS_f) and case C (min $\mu_{0,f}$) in unseeded processes. It is shown that the optimal supersaturation trajectories do not change significantly.
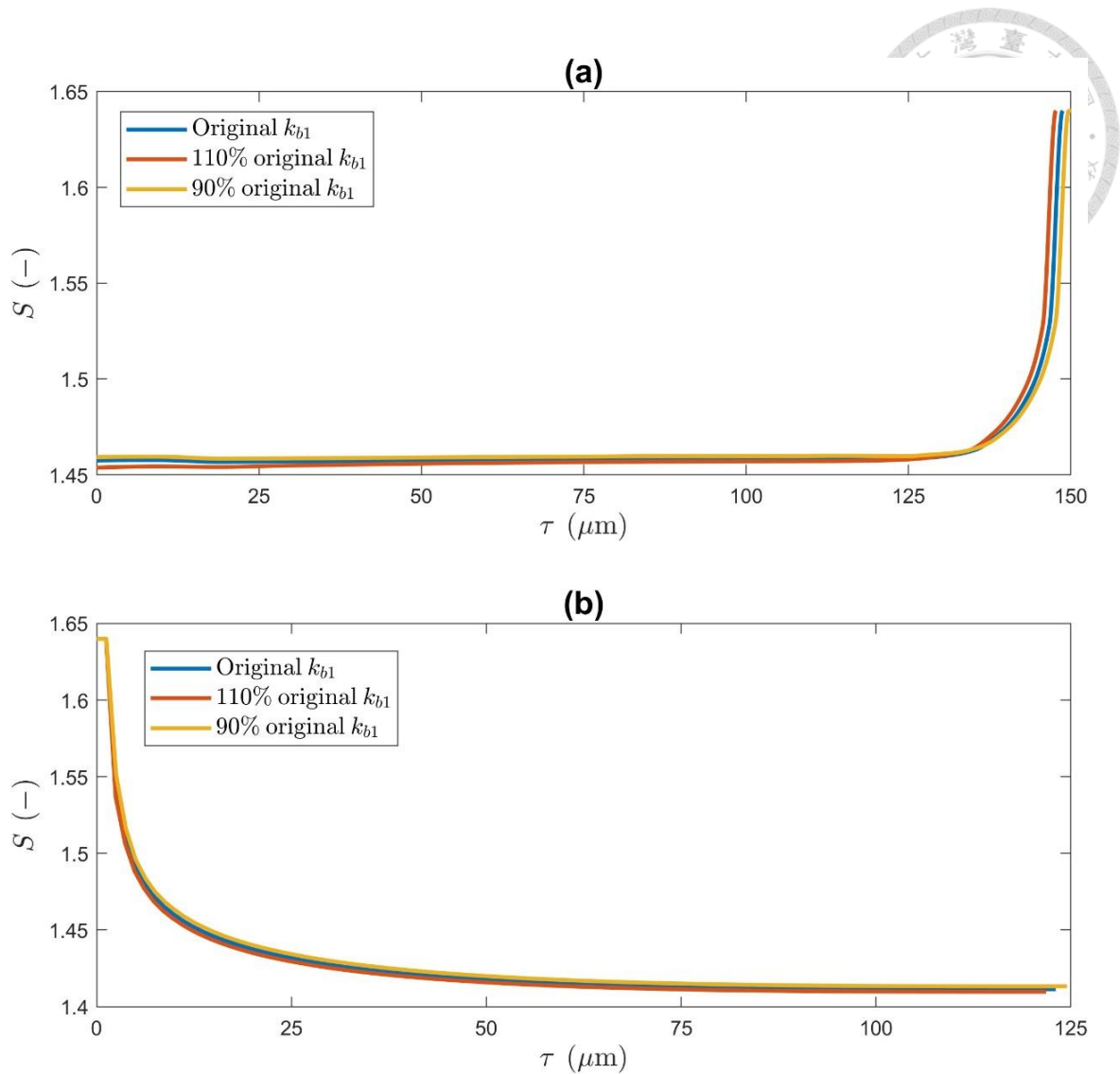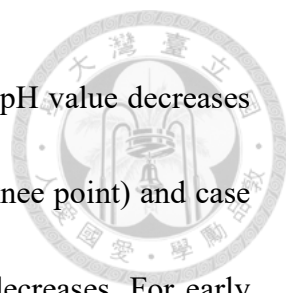
47

Figure 4.6. Results of the sensitivity analysis of primary nucleation rate in unseeded

processes: (a) comparison of supersaturation trajectories for case A (max $\mathbf{WMS_f}$), (b)

comparison of supersaturation trajectories for case C (min $\boldsymbol{\mu_{0,f}}$).

Again after the optimal supersaturation trajectories are determined, the optimal pH

value trajectories can be obtained using Eq 2.31, Eq 2.32, and the solubility data (see

Figure 4.3). The higher the pH value, the higher the solubility. Figure 4.7 shows the results

of optimal supersaturation trajectories and pH value trajectories in time domain. For case

48

A(max WMS_f), a late growth operating policy is preferred, and the pH value decreases from about 7.35 to about 6.00. However, for case B (closest to the knee point) and case C (min $\boldsymbol{\mu_{0,f}}$), the pH value first slightly increases then gradually decreases. For early growth operating policy (case B and case C), because desired supersaturation decreases faster than the concentration C, C_sat should increase, which corresponds to an increase in the pH value. This is the reason that the pH value in case B and case C increases at the beginning of the batch.
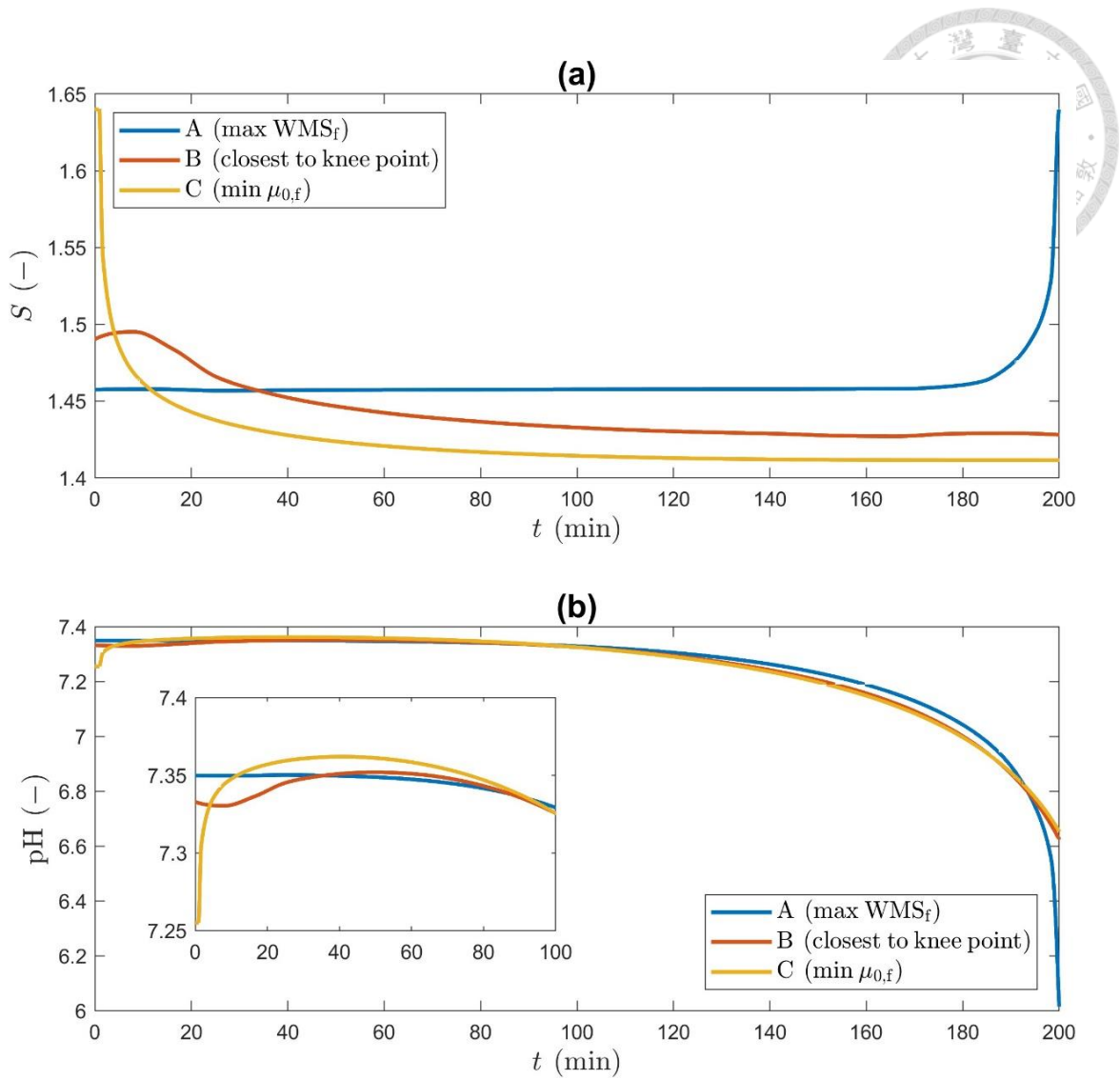
Figure 4.7. Results of optimal control input profiles in time domain in unseeded case:
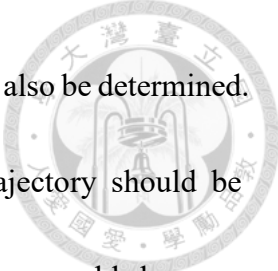
(a) supersaturation trajectories, (b) pH value trajectories.
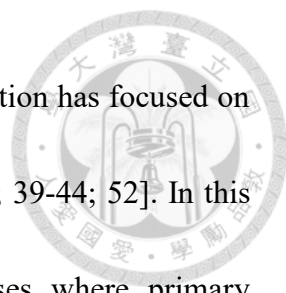
Chapter 5　Conclusions

A framework for multi-objective optimization of seeded and unseeded batch crystallization systems with primary nucleation is developed in this work. The optimization problems are formulated using the method of moments and a time transformation proposed previously[32-36]. Pontryagin's Minimum Principle[37; 38] is used to determine necessary conditions for optimality. Optimization problems are solved efficiently and the complete product CSD is determined. All optimization problems are formulated and solved numerically. For the seeded case, the feedback of nucleation on the system is assumed to be negligible to simplify the expression for the Hamiltonian. For the unseeded case, no such assumption is made and a gradient method[52-54] is applied to solve the challenging TPBVP efficiently. Compared with alternative methods, optimization algorithms based on Pontryagin's Minimum Principle have several advantages, including that they are fast, converge reliably and can be proven to provide the global minimum solution.

For the case study of ampicillin crystallized from water, PFs are constructed to analyze the trade-off between competing objectives. The pH value trajectories, supersaturation trajectories, nucleation rate trajectories, PDFs and VDFs of three optimal solutions on the PF are obtained. With the framework for optimization proposed in this

51

work, optimal operating strategies for different objective functions can also be determined. For example, in the seeded case, a late-growth supersaturation trajectory should be adopted to minimize the nucleus-grown volume in the product. This is reasonable because more nuclei will be formed at the end of the batch and will not have time to grow significantly, which can also be understood clearly from the PDF and VDF. However, a late-growth operating policy will lead to larger number of nucleated crystals.

It is worthwhile to note several limitations of this work. Primary nucleation is difficult to model because it is a stochastic process, and the method proposed here relies on an accurate prediction of the primary nucleation rate. Some authors have proposed stochastic methods for modeling primary nucleation[62-64], however the method described here is limited to the case where there is a deterministic equation such as Equation 2.29 that expresses the primary nucleation rate as a function of the supersaturation. It has also recently been proposed[61] that secondary nucleation is dominant in some situations under high supersaturation where primary nucleation was previously thought to dominate. This possibility should be considered when kinetic models are developed. Finally, as with any optimization algorithm, the algorithm presented here is only as good as the kinetic models upon which it depends. If these models cannot describe the behavior of the process over the range of operating conditions encountered during the optimization, then the optimization results will be unreliable.

Previous work on the application of PMP to batch crystallization has focused on processes with crystal growth and secondary nucleation only[32-36; 39-44; 52]. In this work, primary nucleation is also considered. Therefore, for cases where primary nucleation cannot be neglected, the framework proposed here will be helpful. This work demonstrates that the multi-objective optimization problem can be solved efficiently by PMP using a gradient method to solve the TPBVP. With suitable modifications, the algorithm proposed here might be applied to solve even more complicated and general optimization problems for both seeded and unseeded batch crystallization systems in the future. The moment model has been successfully applied to systems with secondary nucleation when cycles of growth and dissolution are used to tailor the product crystal size distribution[41]. Therefore, this model might be generalized to systems including primary nucleation.
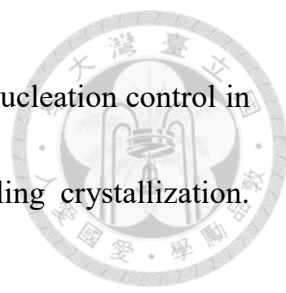
REFERENCES

[1]   Orehek, J., Teslic, D., & Likozar, B. (2020). Continuous crystallization processes in pharmaceutical manufacturing: A review. *Organic Process Research & Development, 25*(1), 16-42.

[2]   Chen, J., Sarma, B., Evans, J. M., & Myerson, A. S. (2011). Pharmaceutical crystallization. *Crystal Growth & Design, 11*(4), 887-895.

[3]   Zhang, D. J., Xu, S. J., Du, S. C., Wang, J. K., & Gong, J. B. (2017). Progress of Pharmaceutical Continuous Crystallization. *Engineering, 3*(3), 354-364. doi: 10.1016/j.Eng.2017.03.023

[4]   Wang, T., Lu, H., Wang, J., Xiao, Y., Zhou, Y., Bao, Y., & Hao, H. (2017). Recent progress of continuous crystallization. *Journal of industrial and engineering chemistry, 54*, 14-29.

[5]   Myerson, A. S., Erdemir, D., & Lee, A. Y. (2019). *Handbook of Industrial Crystallization*: Cambridge University Press.

[6]   Lewis, A., Seckler, M., Kramer, H., & Van Rosmalen, G. (2015). *Industrial crystallization: fundamentals and applications*: Cambridge University Press.

[7]   Ward, J. D., Mellichamp, D. A., & Doherty, M. F. (2006). Choosing an operating policy for seeded batch crystallization. *AIChE Journal, 52*(6), 2046-2054.

[8]   Vekilov, P. G. (2010). Nucleation. *Crystal Growth & Design, 10*(12), 5007-5019.

[9]   Boistelle, R., & Astier, J. (1988). Crystallization mechanisms in solution. *Journal of crystal growth, 90*(1-3), 14-30.

[10]   Lacmann, R., Herden, A., & Mayer, C. (1999). Kinetics of nucleation and crystal growth. *Chemical Engineering & Technology: Industrial Chemistry-Plant Equipment-Process Engineering-Biotechnology, 22*(4), 279-289.

[11]   Agrawal, S., & Paterson, A. (2015). Secondary nucleation: mechanisms and models. *Chemical Engineering Communications, 202*(5), 698-706.

[12]   Hintz, R. J., & Johnson, K. C. (1989). The effect of particle size distribution on dissolution rate and oral absorption. *International Journal of Pharmaceutics, 51*(1), 9-17.

[13]   Meng, W., Sirota, E., Feng, H., McMullen, J. P., Codan, L., & Cote, A. S. (2020). Effective Control of Crystal Size via an Integrated Crystallization, Wet Milling, and Annealing Recirculation System. *Organic Process Research & Development, 24*(11), 2639-2650.

[14]   Abu Bakar, M. R., Nagy, Z. K., Saleemi, A. N., & Rielly, C. D. (2009). The impact of direct nucleation control on crystal size distribution in pharmaceutical crystallization processes. *Crystal Growth and Design, 9*(3), 1378-1384.

[15]   Nagy, Z. K., Chew, J. W., Fujiwara, M., & Braatz, R. D. (2008). Comparative performance of concentration and temperature controlled batch crystallizations. *Journal of Process Control, 18*(3-4), 399-407. doi: 10.1016/j.jprocont.2007.10.006

[16]   Furuta, M., Mukai, K., Cork, D., & Mae, K. (2016). Continuous crystallization using a sonicated tubular system for controlling particle size in an API manufacturing process. *Chemical Engineering and Processing-Process Intensification, 102*, 210-218. doi: 10.1016/j.cep.2016.02.002

[17]   Mesbah, A., Landlust, J., Huesman, A. E. M., Kramer, H. J. M., Jansens, P. J., & Van den Hof, P. M. J. (2010). A model-based control framework for industrial batch crystallization processes. *Chemical Engineering Research & Design, 88*(9A), 1223-1233. doi: 10.1016/j.cherd.2009.09.010

[18]   Acevedo, D., Yang, Y., Warnke, D. J., & Nagy, Z. K. (2017). Model-Based Evaluation of Direct Nucleation Control Approaches for the Continuous Cooling Crystallization of Paracetamol in a Mixed Suspension Mixed Product Removal System. *Crystal Growth & Design, 17*(10), 5377-5383. doi: 10.1021/acs.cgd.7b00860
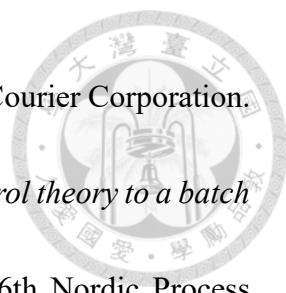
[19]   Yang, Y., Song, L., & Nagy, Z. K. (2015). Automated direct nucleation control in continuous mixed suspension mixed product removal cooling crystallization. *Crystal Growth & Design, 15*(12), 5839-5848.

[20]   Yu, Z. Q., Chow, P. S., & Tan, R. B. (2006). Seeding and constant-supersaturation control by ATR-FTIR in anti-solvent crystallization. *Organic Process Research & Development, 10*(4), 717-722.

[21]   Saleemi, A. N., Rielly, C. D., & Nagy, Z. K. (2012). Comparative investigation of supersaturation and automated direct nucleation control of crystal size distributions using ATR-UV/vis spectroscopy and FBRM. *Crystal Growth & Design, 12*(4), 1792-1807.

[22]   Szilagyi, B., Eren, A., Quon, J. L., Papageorgiou, C. D., & Nagy, Z. K. (2020). Application of model-free and model-based quality-by-control (QbC) for the efficient design of pharmaceutical crystallization processes. *Crystal Growth & Design, 20*(6), 3979-3996.

[23]   Nagy, Z. K. (2009). Model based robust control approach for batch crystallization product design. *Computers & Chemical Engineering, 33*(10), 1685-1691. doi: 10.1016/j.compchemeng.2009.04.012

[24]   Fevotte, F., & Fevotte, G. (2010). A method of characteristics for solving population balance equations (PBE) describing the adsorption of impurities

during crystallization processes. *Chemical Engineering Science, 65*(10), 3191-3198. doi: 10.1016/j.ces.2010.02.009

[25]   Kumar, S., & Ramkrishna, D. (1997). On the solution of population balance equations by discretization—III. Nucleation, growth and aggregation of particles. *Chemical Engineering Science, 52*(24), 4659-4679.

[26]   Lee, G., Meyer, X. M., Biscans, B., Le Lann, J. M., & Yoon, E. S. (1999). Adaptive finite difference method for the simulation of batch crystallization. *Computers & Chemical Engineering, 23*, S363-S366. doi: 10.1016/s0098-1354(99)80089-1

[27]   van Peborgh Gooch, J. R., & Hounslow, M. J. (1996). Monte Carlo simulation of size-enlargement mechanisms in crystallization. *AIChE Journal, 42*(7), 1864-1874.

[28]   Haseltine, E. L., Patience, D. B., & Rawlings, J. B. (2005). On the stochastic simulation of particulate systems. *Chemical Engineering Science, 60*(10), 2627-2641. doi: 10.1016/j.ces.2004.05.038

[29]   Madras, G., & McCoy, B. J. (2002). Dynamics of crystal size distributions with size-dependent rates. *Journal of crystal growth, 243*(1), 204-213.

[30]   Hulburt, H. M., & Katz, S. (1964). Some problems in particle technology: A statistical mechanical formulation. *Chemical Engineering Science, 19*(8), 555-574.

[31]   Randolph, A. (2012). *Theory of particulate processes: analysis and techniques of continuous crystallization*: Elsevier.

[32]   Bajcinca, N. (2013). Analytic solutions to optimal control problems in crystal growth processes. *Journal of Process Control, 23*(2), 224-241. doi: 10.1016/j.jprocont.2012.08.010

[33]   Vollmer, U., & Raisch, J. (2006). Control of batch crystallization—A system inversion approach. *Chemical Engineering and Processing: Process Intensification, 45*(10), 874-885.

[34]   Hofmann, S., Bajcinca, N., Raisch, J., & Sundmacher, K. (2017). Optimal control of univariate and multivariate population balance systems involving external fines removal. *Chemical Engineering Science, 168*, 101-123. doi: 10.1016/j.ces.2016.12.032

[35]   Hofmann, S., & Raisch, J. (2012). Solutions to inversion problems in preferential crystallization of enantiomers-part I: Batch crystallization in a single vessel. *Chemical Engineering Science, 80*, 253-269. doi: 10.1016/j.ces.2012.06.021

[36]   Hofmann, S., & Raisch, J. (2013). Solutions to inversion problems in preferential crystallization of enantiomers-Part II: Batch crystallization in two coupled vessels. *Chemical Engineering Science, 88*, 48-68. doi: 10.1016/j.ces.2012.10.030

[37]   Pontryagin, L. S. (1987). *Mathematical theory of optimal processes*: CRC press.

[38]   Kirk, D. E. (2004). *Optimal control theory: an introduction*: Courier Corporation.

[39]   Hofmann, S., & Raisch, J. (2010). *Application of optimal control theory to a batch crystallizer using orbital flatness.* Paper presented at the 16th Nordic Process Control Workshop, Lund, Sweden.

[40]   Tseng, Y. T., & Ward, J. D. (2017). Comparison of objective functions for batch crystallization using a simple process model and Pontryagin's minimum principle. *Computers & Chemical Engineering, 99*, 271-279. doi: 10.1016/j.compchemeng.2017.01.017

[41]   Pan, H. J., & Ward, J. D. (2021). Computationally Efficient Algorithm for Solving Population Balances with Size-Dependent Growth, Nucleation, and Growth-Dissolution Cycles. *Industrial & Engineering Chemistry Research, 60*(34), 12614-12628. doi: 10.1021/acs.iecr.1c01947

[42]   Pan, H. J., & Ward, J. D. (2021). Dimensionless Framework for Seed Recipe Design and Optimal Control of Batch Crystallization. *Industrial & Engineering Chemistry Research, 60*(7), 3013-3026. doi: 10.1021/acs.iecr.0c06132

[43]   Pan, H. J., & Ward, J. D. (2020). Optimization of Simple Batch Crystallization Systems Considering Crystal Shape and Nucleation. *Industrial & Engineering Chemistry Research, 59*(20), 9550-9561. doi: 10.1021/acs.iecr.9b06842

[44] Tseng, Y. T., Pan, H. J., & Ward, J. D. (2019). Pareto-Optimal Fronts for Simple Crystallization Systems Using Pontryagin's Minimum Principle. *Industrial & Engineering Chemistry Research, 58*(31), 14239-14251. doi: 10.1021/acs.iecr.9b02394

[45] Kubota, N., Doki, N., Yokota, M., & Sato, A. (2001). Seeding policy in batch cooling crystallization. *Powder technology, 121*(1), 31-38.

[46] Aamir, E., Nagy, Z., & Rielly, C. (2010). Evaluation of the effect of seed preparation method on the product crystal size distribution for batch cooling crystallization processes. *Crystal Growth & Design, 10*(11), 4728-4740.

[47] Zhang, C.-t., Wang, H.-r., & Wang, Y.-l. (2010). Internally generated seeding policy in anti-solvent crystallization of ceftriaxone sodium. *Chemical Engineering and Processing: Process Intensification, 49*(4), 396-401.

[48] Zhang, F., Shan, B., Wang, Y., Zhu, Z., Yu, Z.-Q., & Ma, C. Y. (2021). Progress and opportunities for utilizing seeding techniques in crystallization processes. *Organic Process Research & Development, 25*(7), 1496-1511.

[49] He, Y., Gao, Z., Zhang, T., Sun, J., Ma, Y., Tian, N., & Gong, J. (2020). Seeding techniques and optimization of solution crystallization processes. *Organic Process Research & Development, 24*(10), 1839-1849.

[50] Hemalatha, K., Nagveni, P., Kumar, P. N., & Rani, K. Y. (2018). Multiobjective optimization and experimental validation for batch cooling crystallization of citric acid anhydrate. *Computers & Chemical Engineering, 112*, 292-303. doi: 10.1016/j.compchemeng.2018.02.019

[51] Ashraf, A. B., & Rao, C. S. (2022). Multiobjective temperature trajectory optimization for unseeded batch cooling crystallization of aspirin. *Computers & Chemical Engineering, 160*. doi: 10.1016/j.compchemeng.2022.107704

[52] Pan, H.-J., & Ward, J. D. (2023). Algorithms for solving boundary value problems in optimal control of seeded batch crystallization processes with temperature-dependent kinetics. *Chemical Engineering Science, 270*, 118517.

[53] Srinivasan, B., Palanki, S., & Bonvin, D. (2003). Dynamic optimization of batch processes: I. Characterization of the nominal solution. *Computers & Chemical Engineering, 27*(1), 1-26.

[54] Aydin, E., Bonvin, D., & Sundmacher, K. (2017). Dynamic optimization of constrained semi-batch processes using Pontryagin's minimum principle—An effective quasi-Newton approach. *Computers & Chemical Engineering, 99*, 135-144.

[55] Hemalatha, K., & Rani, K. Y. (2017). Multiobjective Optimization of Unseeded and Seeded Batch Cooling Crystallization Processes. *Industrial & Engineering Chemistry Research, 56*(20), 6012-6021. doi: 10.1021/acs.iecr.7b00586

[56] Bhoi, S., Lenka, M., & Sarkar, D. (2017). Particle engineering by optimization for the unseeded batch cooling crystallization of L-asparagine monohydrate. *CrystEngComm, 19*(42), 6373-6382.

[57] Cohon, J. L. (2004). *Multiobjective programming and planning* (Vol. 140): Courier Corporation.

[58] Zelany, M. (1974). A concept of compromise solutions and the method of the displaced ideal. *Computers & Operations Research, 1*(3-4), 479-496.

[59] Bryson, A., & Ho, Y.-C. (1975). Applied optimal control, hemisphere pub. *Corp., Washington DC*.

[60] Encarnación-Gómez, L. G., Bommarius, A. S., & Rousseau, R. W. (2016). Crystallization kinetics of ampicillin using online monitoring tools and robust parameter estimation. *Industrial & Engineering Chemistry Research, 55*(7), 2153-2162.

[61] Hoffmann, J., Flannigan, J., Cashmore, A., Briuglia, M. L., Steendam, R. R., Gerard, C. J., . . . Ter Horst, J. H. (2022). The unexpected dominance of secondary over primary nucleation. *Faraday Discussions, 235*, 109-131.

[62]   Deck, L.-T., & Mazzotti, M. (2022). Conceptual Validation of Stochastic and Deterministic Methods To Estimate Crystal Nucleation Rates. *Crystal Growth & Design*.

[63]   Unno, J., & Hirasawa, I. (2021). Numerical Simulations of Seeded Batch Crystallization Demonstrating the Effect of Stochastic Nucleation on Crystal Product Quality. *Journal of Chemical Engineering of Japan, 54*(7), 380-386.

[64]   Maggioni, G. M., & Mazzotti, M. (2015). Modelling the stochastic behaviour of primary nucleation. *Faraday Discussions, 179*, 359-382.